UNIVERSITY OF GENOA

PhD PROGRAM IN BIOENGINEERING AND ROBOTICS

Controlling the Adipose-derived Stem cell 3D-organization on micrometric PLGA regular scaffolds for cardiac tissue regeneration and repair

Candidate: Federica Grilli

Thesis submitted for the degree of *Doctor of Philosophy* (34°cycle)

Supervisors: Paolo Decuzzi and Daniele di Mascolo

Head of the PhD program: Giorgio Cannata

Dibris

Department of Informatics, Bioengineering, Robotics and Systems Engineering

Declaration

I hereby declare that except where specific reference is made to the work of others, the contents of this dissertation are original and have not been submitted in whole or in part for consideration for any other degree or qualification in this, or any other university. This dissertation is my own work and contains nothing, which is the outcome of work done in collaboration with others, except as specified in the text and Acknowledgements. This dissertation contains fewer than 65,000 words including appendices, bibliography, footnotes, tables and equations and has fewer than 150 figures.

Federica Grilli

31/05/2022

Table of Contents

Chapter 1 7
1.1 Cardiovascular diseases 7
1.2. Clinical presentations and classification of Myocardial Infarction 8
1.3 Guidelines for the management of Myocardial Infarction 12
Emergency care: 12
Reperfusion and adjunctive therapy 13
Fibrinolysis and pharmacoinvasive strategy 13
Coronary Artery Bypass Graft (CABG) surgery 14
Long-term therapy: 14
1.4. Phases of cardiac repair after Myocardial Infarction 16
1.5. Cardiac Stem Cell 17
1.6. Stem-cell based therapy for cardiac regeneration 19
1.7. Therapeutic efficacy of MSCs 22
1.8. Stem cell-based therapy clinical challenges 29
1.9. Bioengineering approaches for improving MSC administration 30
1.10. Aims of the project 33
Chapter 2 35
2.1. Abstract 35
2.2. Introduction 37
2.3. Materials and methods 39
Fabrication of the microMESH 40
microMESH characterization 41
hADSCs interaction with the substrates 42
Single cell suspension from hADSCs spheroids on microMESH 44
hADSCs viability study 45
hADSCs cytoskeleton organization study 46
hADSCs secretome analysis under pro-inflammatory insult 47
hADSCs phenotypic characterization on microMESH 48
Statistics analysis 48
2.4 Results 49
Manufacturing and characterization of microMESH 49
hADSCs interaction with the microMESH 50

Spheroid-derived hADSCs viability analysis 53
Actin reorganization during hADSCs interaction with microMESH 55
Analysis of hADSCs secretome exposed to pro inflammatory stimulus 57
Phenotypic characterization of spheroid-forming hADSCs 60
2.5. Discussion 62
Chapter 3 66
3.1. Conclusions and future outlook 66

List of figures

Figure 1. Schematic of Myocardial Infarction type I. Type I MI is related to ischaemia due to a primary coronary event such as plaque erosion and/or ropture with occlusive or non-occlusive thrombus. 9
Figure 2. Comparison among embolus and thrombus. Thrombus is defined as a blood clot formation in an artery or vein or in stented area. An embolus is a piece of a thrombus that has broken free and is carried toward the circulation by the bloodstream. 9
Figure 3. Schematic of Myocardial Infarction type II. Type II Myocardial infarction is secondary to ischaemia due to either increased oxygen demand or decreased supply. 10
Figure 4. Scheme of the baloon angioplasty procedure. Firstly, **a)** a stent, a wire mesh tube, is compressed over a baloon on the tip of a specially designed catheter and carefully guided along the wire to the artery blockage. Then, **b)** the balloon is inflated and the artery expands, resulting in the lock of the stent in the place. Finally, **c)** the balloon is deflated, and the stent stays in the place to hold the artery open. At the end of the procedure, the guide wire is removed. 12
Figure 5. Multistep procedures for microMESH realization. The top-down fabrication strategy involves different sequential steps. **a)** The first step is the fabrication of a silicon master template via Direct Laser Writing (in grey). Then, a PDMS solution (in light blue) is deposited on top of the silicon template. **b)** The PDMS template is replicated into PVA template by pouring a PVA solution (in yellow) on top of it. Later, **c)** the polymerized PVA template with the same arrays of pillars as the original silicon template is loaded with a polymeric paste of PLGA (in green) to fill up the empty wide strands between the micropillars over the PVA template. PLGA is dissolved in Acetonitrile and spread overall the surface of the PVA template using a blade. Finally, **d)** following ACN evaporation, the final microMESH is released by full dissolution of the PVA component in water. 41
Figure 6. Schematic of the experimental design to study the interaction between hADSCs and the microMESH. a) Placement of the microMESH on the bottom of a plastic dish and cell seeding in separate drops. **b)** Partial dissolution of the PVA backing layer and release of the final microMESH. **c)** Relocation of the microMESH in another Petri dish in order to remove cells not firmly attached to the scaffolds. 43
Figure 7. Overview of the spheroids disaggregation protocol. The schematics show the step-by-step procedure including **a)** hADSCs seeding and their aggregation into spheroids over the microMESH. **b)** Incubation with trypsin and finally, in **c)** spheroids dissociation into single cells, which are later collected in small tubes suspended in culture medium. 45
Figure 8. Geometrical characterization of the microMESH. a) The upper panel shows SEM images of the PVA template of the 5x5, 10x10 and 20x20 geometry. **b)** The middle panel shows from left to right 5x5, 10x10 and 20x20 microMESH, highlighting their peculiar flexibility (scale bar: 50μm). **c)** The bottom panel shows confocal microscopy images of Curcumin-loaded microMESH (green) of the same mentioned geometries. 50
Figure 9. Analysis of spheroids growth over time. a) From left to right SEM images showing the transversal section (left) and the continuous surface (middle) of the collagen scaffold, whilst the fluorescence microscopy image (right) demonstrate cells adhered in 2D monolayer over the collagen sheet**. b)** The fluorescent microscopy image (left) displays the cells arranged into spheroids on top of 20x20 microMESH, whereas SEM images (middle and right) confirms the incorporation of the 20x20 microMESH within the structure of the spheroid. **c)** Spheroids characterization in terms of number of spheroids per microMESH, perimeter and aspect ratio at

different time points, namely 24, 48 and 72h. Data are presented as mean ± SD. Each experiment was repeated multiple times independently (n ≥3). Differences are considered statistically significant when returning a p<0.05 (*), p<0.01 (**) and p<0,0001 (****).....52
Figure 10. Cell viability. hADSCs viability in 2D and 3D cultures at **a)** 24h **b)** 48h and **c)** 72h. Data are presented as mean ± SD. Each experiment was repeated multiple times independently (n ≥3). Differences were considered statistically significant when returning a p value lower than 0.05 (*) and lower than 0.01 (**).....54
Figure 11. hADSCs cytoskeleton organization. a) Confocal microscopy images show cells adhered in 2D monolayer in a Petri dish and on top of a collagen scaffold, and arranged into spheroids over the 5x5, 10x10 and 20x20 microMESH. **b**) Quantification of actin distribution within the cells. * represents a statistical significant difference compared to 2D Petri dish (p<0.05). # represents a statistical significant difference compared to collagen scaffold (p<0.05) (n>3).....57
Figure 12. Analysis of hADSCs secretome exposed to TNF-α stimulation. a) Membrane array in which are underlined the negative (in yellow) and the positive (in red) control spots. **b)** Quantification of the cytokines' expression levels among the different scaffolds at 48h. Data are presented as mean ± SD. Each experiment was repeated multiple times independently (n ≥3). Differences are considered statistically significant when returning a p<0.05 (*) and p< 0.01 (**). 59
Figure 13. Flow cytometry analysis of stemness markers. In order, from left to right the fluorescence associated to CD44, CD90 and CD105 at **a)** 24h, **b)** 48h and **c)** 72h. Each bar represents the mean of almost four repetitions ± SD. Differences are considered statistically significant when returning a p value<0.05 (*), p< 0.01(**), p< 0.001 (***) and p<0.0001 (****)...61

Chapter 1

1.1 Cardiovascular diseases

In the past few decades, the prevalence of Cardiovascular Diseases (CVDs) have increased significantly and become one of the leading causes of mortality throughout the world, including the low-income and middle-income countries [1],[2]. Every year 7.9 million people die from CVDs, an estimated 32% of all deaths worldwide. CVDs, a group of disorders of the heart and blood vessels, are caused by infectious factors and noninfectious factors. Infectious CVDs range from rheumatic heart disease, tuberculous pericarditis, and HIV-induced disease. Whilst noninfectious CVDs include hypertension, myocardial infarction (MI), stroke and peripheral artery disease. Additionally, the incidence of CVDs caused by noninfectious factors, especially ischaemic CVDs, such as MI, is likely to increase in the coming decades [3].

The most important behavioral risk factors of noninfectious CVDs are unhealthy diet, physical inactivity, tobacco use and harmful use of alcohol. The effects of behavioral risk factors may manifest in individuals as raised blood pressure, raised blood glucose level, raised blood lipids concentration, an increase in body weight and/or obesity. These “intermediate risks factors” can be measured in primary care facilities and indicate an increased risk of myocardial infarction, stroke and heart failure (HF), the end-stage of many heart diseases [4]. Thus, the cessation of tobacco use, reduction of salt in the diet, eating more fruit and vegetables, regular physical activity and avoiding copious use of alcohol have been shown to reduce the risk of CVDs. Health policies that create favorable environments for making healthy choices affordable and available are essential for motivating people to adopt and sustain healthy behaviors.

Identification and timely treatment of CVD risk factors is currently the key strategy for reducing CVDs prevalence in populations [5],[6],(http://www.who.int/cardiovascular_diseases/en/).

The heart contains many cell types among which: atrial cardyomyocites, ventricular cardyomyocites, fibroblasts (FBs), Endothelial Cells (ECs), perycites, Smooth Muscle Cells (SMCs), immune cells, adipocytes, mesothelial cells and neuronal cells. Cardyomyocites (CMs) are the most prevalent cardiac cells with a higher percentage in ventricular than in atria [7].

Acute myocardial injury can kill as many as 25% of CMs from the left ventricle, corresponding to up to 1 billion cells [8]. MI can ultimately develops into heart failure, to which the heart transplantation is the only resolute therapy, although is severely limited by critical donor's shortage. HF is a leading cause of hospitalization, adverse quality of life, and death and a new diagnosis carries a worse prognosis than several common cancers [9]. Thus, the need to develop novel therapies for MI to prevent heart failure is impelling [2],[5],[10],[11],[12],[13].

1.2. Clinical presentations and classification of Myocardial Infarction

MI is defined pathologically as myocardial cell death due to prolonged ischaemia, which results from an imbalance between oxygen supply and demand. Myocardial ischaemia in a clinical setting can most often be identified from the patient's history and from the echocardiogram. Possible ischaemic symptoms include various combinations of chest, upper extremity, mandibular, or epigastric discomfort during exertion or at rest, or dyspnea or fatigue. Often, the discomfort is diffuse; not localized, nor positional, nor affected by movement of the region. However, these symptoms are not specific for myocardial ischaemia and can be observed in other conditions such as gastrointestinal, neurological, pulmonary, or musculoskeletal complaints. Additionally, MI may occur with atypical symptoms such as palpitations or cardiac arrest, or even without symptoms. MI can be classified into various types based on pathological, clinical, and prognostic differences [14].

Type I MI

MI caused by atherothrombotic coronary artery disease (CAD) and usually precipitated by atherosclerotic plaque disruption (rupture or erosion) is designated as a type I MI (**Fig.1**).

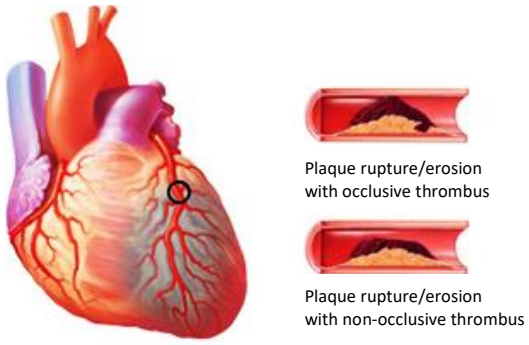

Figure 1. Schematic of Myocardial Infarction type I. Type I MI is related to ischaemia due to a primary coronary event such as plaque erosion and/or ropture with occlusive or non-occlusive thrombus.

The relative burden of atherosclerosis and thrombosis in the damaged lesion varies greatly, and the dynamic thrombotic component may lead to distal coronary embolization resulting in myocyte necrosis. Plaque rupture may not only be complicated by intraluminal thrombosis but also by hemorrhage into the plaque through the disrupted surface (**Fig.2**).

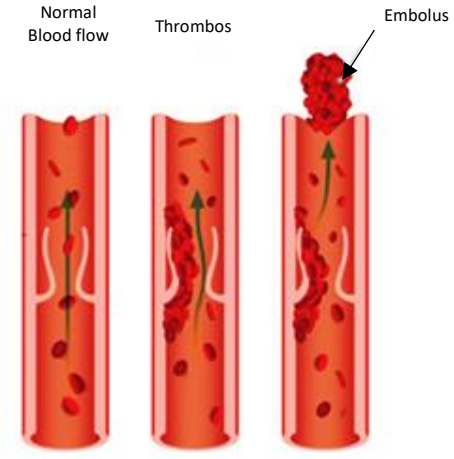

Figure 2. Comparison among embolus and thrombus. Thrombus is defined as a blood clot formation in an artery or vein or in stented area. An embolus is a piece of a thrombus that has broken free and is carried toward the circulation by the bloodstream.

Type II MI

The pathophysiological mechanism leading to ischaemic myocardial injury in the context of a mismatch between oxygen supply and demand has been classified as type II MI (**Fig.3**). The myocardial oxygen supply/demand imbalance attributable to acute myocardial ischaemia may be multifactorial, related either to a:

- reduced myocardial perfusion due to fixed coronary atherosclerosis without plaque rupture, coronary artery spasm, coronary microvascular dysfunction (which includes endothelial dysfunction, smooth muscle cell dysfunction, and the dysregulation of sympathetic innervation), coronary embolism, coronary artery dissection (with or without intramural hematoma) or other mechanisms that reduce oxygen supply, such as severe bradyarrhythmia, respiratory failure and hypotension/shock;
- increased myocardial oxygen demand due to sustained tachyarrhythmia or severe hypertension with or without left ventricular hypertrophy.

.

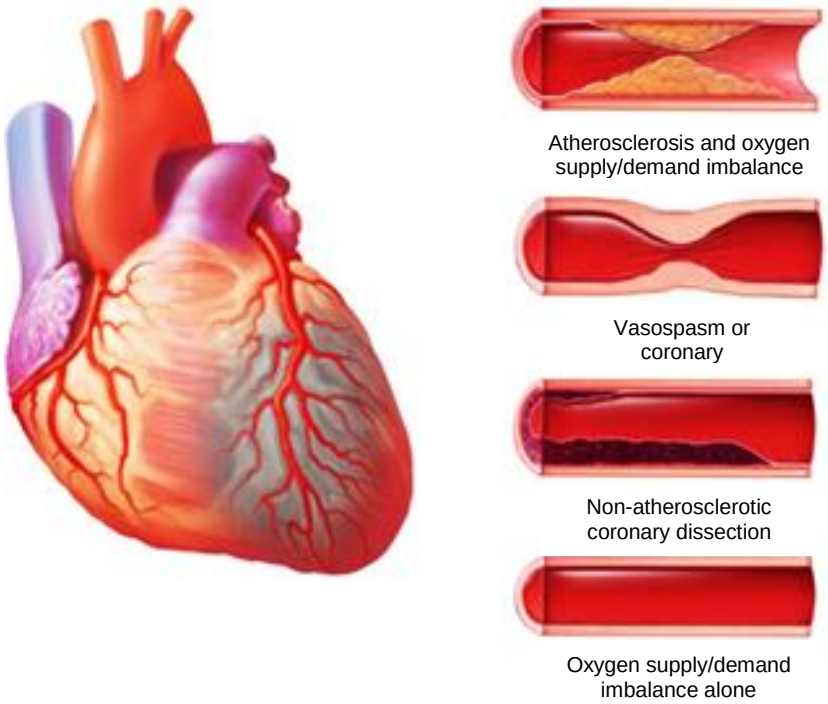

Figure 3. Schematic of Myocardial Infarction type II. Type II Myocardial infarction is secondary to ischaemia due to either increased oxygen demand or decreased supply.

Type III MI

The detection of cardiac biomarkers in the blood is fundamental for establishing the diagnosis of MI. However, patients can manifest a typical presentation of myocardial ischaemia/infarction, and die before it is possible to obtain blood for cardiac biomarker determination; either the patient may die soon after the onset of symptoms before an elevation of biomarker values has occurred. Such patients are designated as having a type III MI, when suspicion for an acute myocardial ischaemic event is high, even when cardiac biomarker evidences of MI is lacking. This category divides fatal MI events from the much larger group of sudden death episodes that may be cardiac (non-ischaemic) or non-cardiac in origin.

Type IV and V MI

Type IV and V MI are procedure-related. Myocardial injury related to coronary revascularization procedures, whether Percutaneous Coronary Intervention (PCI) or Coronary Artery Bypass Grafting (CABG), may be concerned to the procedure itself or may occur later, reflecting complications of a device, such as early or late stent thrombosis or in-stent restenosis for PCI, or graft occlusion or stenosis for CABG procedure. Type IV MI is associated with percutaneous coronary intervention (IV A) or stent/scaffold thrombosis (IV B). Occasionally MI occurs in restenosis, a re-narrowing or blockage of the culprit region, following balloon angioplasty in the infarct territory (**Fig.4**). This PCI-related MI type is designated as type IV C. Finally, MI type V is related to Coronary Artery Bypass Grafting (CABG) surgery [14].

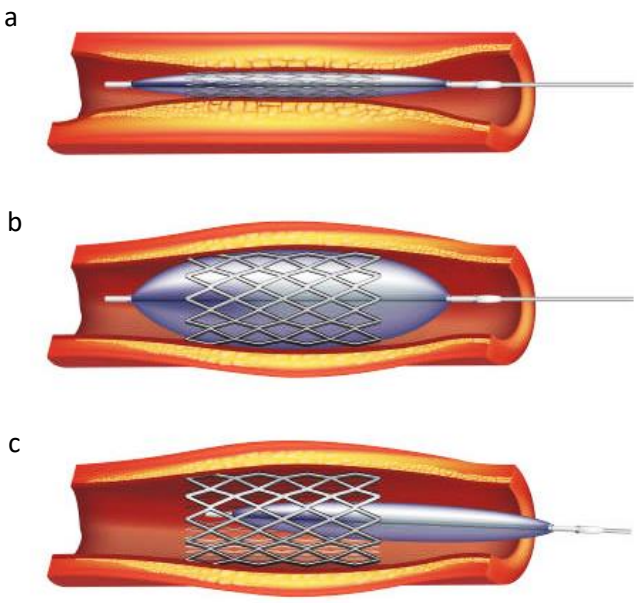

Figure 4. Scheme of the baloon angioplasty procedure. Firstly, **a)** a stent, a wire mesh tube, is compressed over a baloon on the tip of a specially designed catheter and carefully guided along the wire to the artery blockage. Then, **b)** the balloon is inflated and the artery expands, resulting in the lock of the stent in the place. Finally, **c)** the balloon is deflated, and the stent stays in the place to hold the artery open. At the end of the procedure, the guide wire is removed.

1.3 Guidelines for the management of Myocardial Infarction

Management—including treatment—of MI starts from the first medical contact that can be either in the prehospital setting or upon patient arrival at the hospital (e.g. emergency department).

Emergency care:

It includes: **1)** analgesics due to the fact that the relief of pain is of paramount importance, not only for comfort reasons rather because the pain is associated with sympathetic nervous system activation, which causes vasoconstriction and increases the workload of the heart. Titrated intravenous opioids (e.g. morphine) are the analgesics most commonly used in this context.

However, the use of morphine is associated with a slower uptake, delayed onset of action, and diminished effects of oral antiplatelet agents (e.g. clopidogrel, ticagrelor, and prasugrel), which may lead to early treatment failure in susceptible individuals. Further, **2)** oxygen when the patient presents an arterial oxygen saturation <90%. Finally **3)** a mild tranquillizer (usually a benzodiazepine) should be considered in anxious patients. Anxiety is a natural response to the pain and the circumstances surrounding MI. Thus, reassurance of patients and those closely associated with anxiety is of great importance [15].

Reperfusion and adjunctive therapy

Primary PCI is the preferred reperfusion strategy in patients with MI. Among others (e.g. thrombus aspiration, multivessel coronary revascularization, intra-aortic balloon pump), coronary stenting is the technique of choice during primary PCI.

Patients undergoing primary PCI should receive a Dual Anti-Platelet Therapy (DAPT): a combination of aspirin and a P2Y12 inhibitor, and a parenteral anticoagulant. The preferred P2Y12 inhibitors are prasugrel or ticagrelor. Whereas, anticoagulant options include Unfractionated Heparin (UFH), enoxaparin, and bivalirudin [16].

Fibrinolysis and pharmacoinvasive strategy

Fibrinolytic therapy is an important reperfusion strategy in settings where primary PCI can not be offered in a timely manner. Precisely, fibrinolytic therapy is recommended within 12 h of symptom onset if primary PCI can not be performed within 120 min from MI diagnosis. After 3h from symptoms onset a more consideration should be given to transfer for primary PCI (as opposed to administering fibrinolytic therapy) because the efficacy and clinical benefits of fibrinolysis

decrease as the time from symptom onset increases. In the presence of contraindications for fibrinolytic treatment, it is important to weigh the potentially life-saving effect of fibrinolysis against potentially life-threatening side effects, taking into account alternative treatment options such as delayed primary PCI. Thus, in cases of failed fibrinolysis, immediate angiography and rescue PCI is indicated (pharmacoinvasive strategy). Weight-adjusted intravenous tenecteplase (fibrinolytic agent), aspirin (anti-platelet agent), and clopidogrel given orally, and enoxaparin intravenous followed by subcutaneous administration until the time of PCI, comprise the antithrombotic cocktail most extensively studied as part of a pharmacoinvasive strategy [16].

Coronary Artery Bypass Graft (CABG) surgery

CABG should be considered for patients with unsuitable anatomy for PCI. It involves taking blood vessels from another part of the body and attaching them to the coronary artery above and below the narrowed area. This creates a new route for the supply of blood to the heart. CABG alleviates symptoms of chest pain and reduce the risk of a first or consequent MI.

Long-term therapy:

It comprises:

- Lifestyle interventions including cessation of smoking, optimal blood pressure control, diet advice and weight control, and physical activity. Detailed recommendations are available from the European Society of Cardiology (ESC) guidelines on prevention [17];
- Anti-thrombotic treatment: low aspirin doses (75–100 mg) are indicated due to similar anti-ischaemic and less adverse events than higher doses, as demonstrated in the CURRENT-OASIS 7 trial [18];

- Beta-blockers administration: early administration of intravenous beta-blockers (e.g. metoprolol) at the time of presentation should be administrated in patients undergoing primary PCI with no signs of acute heart failure. Otherwise, oral beta-blockers should be considered within the first 24h. Calcium channel antagonists (e.g. verapamil) are a reasonable option for patients with contraindications to beta-blockers;

- Lipid-lowering therapy: the benefits of statins in secondary prevention have been unequivocally demonstrated [19]. It is recommended to start high-intensity statins therapy (atorvastatin and simvastatin) as early as possible, unless contraindicated, and maintain it long-term. In patients known to be intolerant of any dose of statin, treatment with ezetimibe, a cholesterol absorption inhibitor should be considered. Statins, known as hydroxy-methyl-glutaryl coenzyme A (HMG-CoA) reductase inhibitors, reduce the plasma LDL-cholesterol levels;

- Angiotensin-Converting Enzyme (ACE) inhibitors and angiotensin II receptor blockers (ARBs) administration: ACE inhibitors are recommended in patients with evidence of heart failure. Patients who do not tolerate an ACE inhibitor should be given an angiotensin II receptor blocker (ARB). Particularly, valsartan (ARB) was found to be non-inferior to captopril (ACE inhibitor) in the VALsartan In Acute myocardial iNfarcTion (VALIANT) trial;

- Mineralocorticoid receptor antagonist (MRA) therapy: it is recommended in patients with heart failure after MI. Eplerenone, a selective aldosterone receptor antagonist, has been shown to reduce morbidity and mortality in these patients acting as an anti-hypertensive [16].

1.4. Phases of cardiac repair after Myocardial Infarction

Mammalian heart use both innate and adaptive immune systems to respond to tissue injury resulting from pathogens or environmental injury (e.g. ischaemia) [20]. Whereas the innate immune system provides a global, nonspecific guard against pathogens or tissue injury, the adaptive immune system provides a highly specific response mediated by T cells and B cells. Myocardial injury initiate a fine orchestrated and complex series of events. The first one is an intense inflammation and immune cell infiltration (inflammatory phase), followed by a reparative phase with the resolution of inflammation. Early inflammatory activation induced by the innate immune system is a necessary event for the transition to the following reparative and proliferative programs. Appropriate and timely containment and resolution of inflammation are further determinants for the quality of wound healing. However, an inflammatory phase - disproportionately prolonged, of excessive magnitude, or insufficiently suppressed- can lead to sustained tissue damage, improper healing, inadequate scar formation, intensified cell loss and contractile dysfunction. Thereby promoting infarct expansion, adverse remodeling, and heart failure [21],[22]. The extent of inflammation correlates with the severity of HF. Thus, a proper physiological balance needs to be achieved between these 2 phases for optimal repair [23].

The early inflammatory phase after MI starts when oxidative stress and the death of tissue, particularly apoptotic and necrotic CMs, trigger the inflammatory response characterized by increased production of pro-inflammatory cytokines and chemokines, accompanied by the rapid influx of neutrophils and monocytes from the circulation to the infarct area. This is subsequently followed by reparative and proliferative phase of resolution, characterized by the phagocytic removal of necrotic cells by macrophages, the influx of T cells (including T helper (TH) cells and regulatory T (Treg) cells) and B cells, the generation of anti-inflammatory mediators (e.g. Transforming Growth Factor β1 (TGF-β1) and IL-10), the formation of new vessels to restore the blood supply and the transition of cardiac fibroblasts into activated myofibroblasts [23].

Myofibroblasts have characteristics of fibroblasts and smooth muscle cells. Indeed, they can contract and produce extra cellular matrix (ECM), a cell-free three-dimensional (3D) scaffold that provides structural integrity and biochemical and biomechanical signaling cues to surrounding cells. In so doing myofibroblasts contribute to tissue replacement and interstitial fibrosis following cardiac injury [23]. The scar formed after the myocardial injury is no longer considered a passive tissue; in fact, it is an active playground where myofibroblasts play a role in the deposition of ECM and scar contraction. Scar formation is critical to protect the heart from life-threatening complications, such as aneurysm formation and cardiac rupture, yet it boosts progressive adverse remodeling, often resulting in ventricle dilation and failure [6],[9],[21],[22],[24],[25],[26],[27].

1.5. Cardiac Stem Cell

Myocardial fibrosis of the infarcted heart causes ventricular remodeling after MI, which represents a major cause of infarct-related HF and death. Despite scientific progresses and advancements in pharmaceutics and surgical techniques, drugs and surgery can only delay the progression of heart disease. However, they can not save the function of infarcted CMs. In fact, the CMs lost during MI can not be regenerated. This belief has been based on the generally accepted notions that **1)** in the adult heart all cardiomyocytes are terminally differentiated and, therefore, can not be reversed into a pluripotent phenotype, and that **2)** the myocardium lacks a stem cell population able to generate new cardiomyocytes. Thus, according to this, the adult mammalian heart should possess a relatively constant number of cardiomyocytes from shortly after birth to adulthood and senescence [28]. However, an increasing number of studies have recently reported an alternative point of view, by which most adult mammalian tissues, as well as the heart, contain a population of undifferentiated cells with many of the characteristics of stem cells. These cells, under the appropriate conditions, are able to reconstitute many or all the cell types of the tissue of origin. Although the molecular mechanism(s) responsible for determining the developmental choice of

these stem cells remains to be elucidated, it soon became evident that damage of the host tissue was a potent stimulus to coach these cells to adopt the fate of the host organ [28]. The recognition that a pool of cardiac stem and progenitor cells (CSCs) resides in the myocardium and that these cells form new myocytes, smooth muscle cells and endothelial cells [29] has provided a different perspective concerning the biology of the heart and the mechanisms of myocardial homeostasis and tissue repair. The new paradigm implies that cardiomyocytes are no longer considered cells that are created only during embryonic and fetal development so that their total number in the heart is established at birth and no further growth occurs post-natally, in adulthood, or during senescence. This paradigm refutes the belief that all cardiomyocytes have the same age and that the age of these cells corresponds to the age of the organ and organism. Similarly, this paradigm suggests that there is a subpopulation of newly born myocytes that result from CSCs differentiation, although most myocytes in the adult heart are terminally differentiated and incapable of re-entering the cells cycle. This myocytes renewal is an essential component of myocardial cell homeostasis [30]. Thus, a new conceptual framework of the heart has emerged. The heart is now viewed as a partially self-renewing organ, in which cardiomyocytes regeneration occurs throughout the organism lifespan [28],[29],[31].

Resident CSCs are stored in a specialized environment known as niche [32]. The niches control the turnover of myocardial cells and the growth, migration, and commitment of progenitor cells, which leave the niches to replace old, dying cells in the myocardium. Thus, stem cell niches are functionally important because they provide a regulatory structure for stem cells, thereby controlling and balancing self-renewal and differentiation. Regeneration after an injury implies that dead cells are replaced by newly formed cells that differentiate and organize in a complex pattern, restoring the original structure of the lost tissue. However, the presence of these putative resident cardiac stem cells, is not enough to reconstitute the CMs lost resulting after coronary artery occlusion, as in the case of MI [1],[29]. The concept of the cardiac stem cell niche is valuable in conceptualizing why the heart does not fully heal itself following tissue necrosis: the process of

tissue disruption destroys not only adult CMs, but also the niches [33]. In addition, tissue-specific stem cells can not be considered as isolated entities; in *vivo* they strictly depend on the interaction with the surrounding environment [32].

Based on these considerations, several clinical attempts were based on the injection, into the infarcted or failing heart, of a wide variety of cell types as a tool to improve cardiac repair and regeneration after MI.

1.6. Stem-cell based therapy for cardiac regeneration

One of the first cell-based cardiac regeneration strategies was the injection of autologous skeletal myoblasts into ischaemic myocardium. It was hoped that these muscle cell progenitors would differentiate into CMs, but they did not. However, the functional improvement by skeletal myoblasts in preclinical studies motivated their testing in patients. Unfortunately, enthusiasm for skeletal myoblast therapy has been tempered by a lack of experimental evidence for true CMs differentiation. Somewhat, myoblasts, when transplanted into an infarcted scar differentiated into myotubes and retained skeletal muscle proprieties [28],[34]. Moreover, it appeared that the implanted cells were not electrically integrated with the host myocytes, which might explain the association with cardiac arrhythmias in early clinical studies [35]. Latest works were performed using stem cells recovered from the bone marrow, namely the Bone Marrow-derived Mononuclear Cells (BM-MNCs), on which are focused most of the study on cell therapy in Acute Myocardial Infarction (AMI).

Strauer *et al* were the first to report that intracoronary infusion of BM-MNCs substantially improves Left Ventricular (LV) function in patients with AMI [36]. Assmus *et al.* obtained similar observations on the twenty patients recruited in the TOPCARE-AMI trial in 2002 [37],[38],[39]. Twenty-four hours after AMI, the patients were randomly assigned to receive intracoronary infusion of bone marrow-derived (n=9) or blood-derived progenitor cells (n=11). The results of the study

demonstrated that intracoronary infusion of both cell types improved the ventricular function due to stimulated neo-angiogenesis, preventing late myocardial remodeling through enhanced myocardial blood, thereby limiting myocyte apoptosis and reducing the scar formation [37]. Moreover, based on the meta-analysis realized by Fischer and colleagues, treatment with BM-MNCs would increase Left Ventricular Ejection Fraction (LVEF) after AMI by 2.72% [40]. Despite most of the knowledge about stem-cell therapy derived from BM-MNCs, several studies on the Mesenchymal Stem Cells (MSCs) are quite encouraging too. Indeed, in the Transendocardial Autologous Mesenchymal Stem Cells and Mononuclear Bone Marrow Cells in Ischemic Heart Failure (TAC-HFT) trial it was demonstrated the safety of transendocardial stem cell injection with autologous MSCs and BM-MNCs in patients with ischaemic cardiomyopathy. The TAC-HFT study was designed to provide a rigorous safety assessment employing two leading candidates for cell-therapy: bone marrow-derived mesenchymal stem cells and bone marrow mononuclear cells. Particularly, 33 patients were randomized to receive mesenchymal stem cells treatment and 32 patients to receive bone marrow cells treatment. Transendocardial injection of both cell types was not associated with an increased risk of adverse side effects. Additionally from the study emerged that MSCs exert regenerative and anti-fibrotic effects within the myocardium and that these effects were associated with improved functional capacity and quality of life [41]. Based on these findings, it seems that MSCs were more efficient for regenerative therapeutic approaches in cardiology. Moreover, the meta-analysis of Fischer and colleagues revealed that treatment with BM-MNCs would increase left ventricular ejection fraction after AMI by 2.72% compared to the increase of 3.67% obtained with MSCs administration [42],[43].

Furthermore, in the POSEIDON trial, it was demonstrated that transplanted allogenic MSCs was as safe and effective as autologous ones. In the study, thirty-one patients were enrolled to receive allogenic or autologous MSCs treatment. The results showed that both cell types were safe, demonstrating potential regenerative activity in ischaemic cardiomyopathy, particularly by

reducing infarct size and improving cardiac remodeling. All these evidences strongly support the development of allogenic MSCs-based therapies [44].

Mesenchymal stem cells are multipotent adult stem cells capable of self-renewal and able to differentiate into different cell types [45],[46]. In the late 1970s, Friedenstein and colleagues, first described an adherent and non-hematopoietic cell type present in the mouse bone-marrow that could form fibroblast-like colonies *in vitro*, now known as Mesenchymal Stem Cells [47],[48]. Despite bone-marrow continues to be the most commonly studied MSC source in preclinical and clinical studies, MSCs can also be isolated from many tissues beyond bone marrow, including adipose tissue, umbilical cord, Wharton's jelly and the placenta [49],[50],[51].

In 2006, the International Society of Cell and Gene Therapy (ISCT) proposed the minimum criteria for defining human mesenchymal stem cells (hMSCs). Firstly, these cells are plastic adherent and have a fibroblast-like morphology. Secondly, they express CD73, CD90, and CD105 but lack the expression of CD34, CD45, CD14 or CD11b, CD79α or CD19, class II major histocompatibility complex (MHCII) molecule (mainly HLA-DR) and co-stimulatory molecules such as B7-1, B7-2, CD80, CD86, CD40 and CD40L. Lastly, they differentiate into cells of the mesodermal lineage, such as adipocytes, osteoblasts, and chondrocytes *in vitro*. [42],[52],[53]. In 2019, ISCT updated its criteria for defining MSCs to include **1)** tissue-source origin of the cells, which would highlight tissue-specific properties and **2)** associating functional assays to define their relevant therapeutic modes of action [54]. Rather, MSCs from different sources exhibit differences in immunophenotype, differentiation potential, transcriptome, and immunomodulatory activity which led to different clinical applications of MSCs [3].

1.7. Therapeutic efficacy of MSCs

MSCs have received much attention in the therapy of CVDs owing to their positive effects, such as reduction in scar size, improved cardiac contractility, and increased tissue perfusion in numerous preclinical studies. While it is still unclear how MSCs elicit these effects, proposed mechanisms have included their paracrine activity, meaning the secretion of pro-angiogenic, anti-fibrotic and anti-apoptotic factors [55], differentiation potential into new cardiomyocytes [56], ability to fuse with host cardiomyocytes [57] and activation of endogenous cardiac stem cells [58]. The relative significance of these mechanisms is widely debated, and the exact biomolecular pathway responsible for the therapeutic effects remain to be fully elucidated.

Heterocellular co-culture studies offer a versatile experimental setting to track the fate and function of individual cells *in vitro*, since the direct, real-time studies of cardiomyocyte/non-cardiomyocyte interactions *in situ* are very difficult to perform [59]. Spontaneous permanent cell fusion between CMs and non-CMs has been observed *in vitro* and *in vivo*. Recently, co-cultures of hMSCs and neonatal rat ventricular myocytes (NRVMs) were performed, from which was demonstrated that the fusion process occurs over a period of hours and leads to the formation of initially contractile cells that progressively lose ordered sarcomeric structures and their ability to contract, and attain electrical properties in between those of passive hMSCs and active NRVMs [59]. Nevertheless, a wide variety of studies proved that MSCs can differentiate into CMs without physical contacts with CMs even if the molecular signals that underlie this process are not fully understood [60]. Anyway, in the work conducted by Zeng et al.in 2008, MSCs isolated from adult rats were co-cultured with CMs obtained from neonatal rat ventricles at 1:5 ratio in a dual chamber dish separated by a semipermeable membrane for 2 weeks. During this non-direct contact co-culture procedure, cardiomyogenic differentiation and relative genes expression in MSCs were evaluated. After having been co-cultured with CMs, MSCs showed a stick-like or elliptical morphology, connected with adjoining cells and aligned in a striated pattern. Immunofluorescent

staining analyses revealed that α-actin and cardiac troponin T positive cells were found in MSCs at 5 days after co-culture with CMs, and these positive cells reached the peak at 14 days. Moreover, the RT-PCR results demonstrated that the expression level of TGF-β, Nkx-2.5, GATA-4 and MEF-2C genes, which are known to play a crucial role during heart development, began to increase at 1 day and reached the peak at 7 days after co-culture [60].

Several groups of researchers have shown that ADSCs, similarly to MSCs, exhibit the same properties to differentiate *in vivo* into cells that exhibit features of cardiac myocytes [61],[62]. Additionally, Planat-Benard et al. in their study demonstrated that ADSCs spontaneously differentiate into cells with morphological, molecular, and functional properties of cardiomyocytes [63],[64]. All these evidences suggest that ADSCs have the potential to promote improvement of cardiac function after acute myocardial infarction (AMI). Nevertheless, researchers, firstly attracted by the self-renewal capacity of MSCs and their differentiation, focused secondarily on the ability of MSCs to regulate immune response and investigated more in this direction. MSCs exert their immunomodulatory effects by secreting a variety of trophic factors with autocrine and paracrine signaling and by interacting with both the innate and adaptive immune cells [48],[65],[66].

MI is intrinsically associated with the activation of an inflammatory reaction, which serves as a protective response to preserve host integrity. Within hours after the onset of an inflammatory response, Toll-Like Receptors (TLRs) present on innate effector cells recognize molecules associated with tissue damage. TLR ligation triggers phagocytosis and the release of inflammatory mediators, which may initiate an innate immune response [67]. TLR ligation may not only activate phagocytic cells (macrophages and neutrophils) but also MSCs, resulting in a development of an inflammatory environment [68]. MSCs express on their surface several TLRs and following TLRs stimulation respond with different immunomodulatory effects and distinct secretomes [69].

MSCs are sensors of inflammation and can adopt a pro-inflammatory or anti-inflammatory phenotype in response to environmental cues, both *in vitro* and *in vivo* [70],[71]. In the presence of an inflammatory environment (high levels of TNF-α and IFN-ɣ), MSCs become activated and adopt an immune-suppressive phenotype (MSC2) by secreting high levels of soluble factors, including, among others, TGF-β1 and Hepatocyte Growth Factor (HGF) that suppress T cell proliferation.

In the absence of an inflammatory environment (low levels of TNF-α and IFN-ɣ), MSCs may adopt a pro-inflammatory phenotype (MSC1) and enhance T cell responses by secreting chemokines (e.g. RANTES and MIP) that recruit lymphocytes to the sites of inflammation, further increasing the inflammation [72],[73].

Within the innate immune system, macrophages are key players in initiating and controlling inflammation, and MSCs can influence macrophage functions depending on the inflammatory context [74],[75]. Based on the specific microenvironment of MSCs, macrophages can be educated to adopt an inflammatory M1 or anti-inflammatory M2 phenotype [76]. MSCs produce constitutively IL-6, which polarizes monocytes (M0), arrived from circulation, toward anti-inflammatory M2 macrophages. Infiltration of monocyte-derived macrophages to the damaged area is a key feature of MI. M2 macrophages secrete a combination of cytokines (including high levels of IL-10 and TGF-β1 and low levels of IL-6, TNF-α, and IFN-ɣ) that together exert an anti-inflammatory effect and allow tissue regeneration following inflammation. The polarizing effect of MSCs on M2 macrophages is closely linked to their ability to favor the emergence of regulatory T cells (Tregs) which are involved in immune-suppression. The emergence of Tregs can be also supported by MSCs directly *via* the production of TGF-β1, which is constitutively secreted by MSCs [71].

On the other hand, in the absence of IL-6, MSCs induce the polarization of M0 toward pro-inflammatory M1 macrophages, which stimulate local inflammation by releasing pro-inflammatory

cytokines, such as TNF-α and IFN-ɣ and promote T cells activation which secrete high level of TNF-α and INF-ɣ that further enhance the inflammation. Interestingly, high levels of pro-inflammatory signals, including TNF-α and IFN-ɣ produced by M1 macrophages or activated T cells act as a feedback mechanism and trigger the release of mediators by MSCs that skew the differentiation of monocytes toward an anti-inflammatory profile [71]. The balance between these opposing pathways may serve to promote host defense on one hand, at the same time create a loop that prevents excessive tissue damage and promote repair.

Excessive activation of M1 macrophages and delayed transition from M1 to M2 dampen the resolution of inflammation and worsen the healing state at the site of injury [77]. Thus, the macrophages polarization provides a supplementary mechanism to maintain the balance between pro-inflammatory and anti-inflammatory effects. This dynamic regulatory feedback between MSCs and macrophages generates a profound sensitivity to the surrounding microenvironment displayed through the ability to switch between pro-inflammatory and anti-inflammatory activities [71],[73]. The pro-inflammatory activities of MSCs may be beneficial in the early phase of inflammation and help in mounting a proper immune response. In contrast, when exposed to sufficient levels of pro-inflammatory cytokines, MSCs may respond by adopting an immune-suppressive (MSC2) phenotype to dampen inflammation and promote tissue homeostasis through polarization toward anti-inflammatory cells and M2 macrophages *in vitro.*

The adaptive immune system is antigen-specific and allows the development of immunological memory. T cells constitute an active group of adaptive immune cells [78] and comprise T helper and T cytotoxic cells that deliver a tailored antigen-specific immune response following antigen processing and presentation by antigen-presenting cells (APCs). T helper cells comprise a subpopulation of cells, namely T regulatory cells (Tregs). Several studies have documented the ability of MSCs to polarize T cells toward a regulatory phenotype [79], that serves as another

important mechanism by which MSCs dampen inflammation. Indeed, MSCs are not constitutively inhibitory, but they need to be primed by inflammatory cytokines in the host to become immunosuppressive [49].

Effector B cells have a central role in the adaptive immune response to antigens *via* their differentiation into plasma cells for antibody production or into memory B cells for enhanced recall response to an antigen. MSCs have demonstrated the ability to regulate the B cell populations by inducing the regulatory B cell (Bregs) production and expansion. The central mediator of Bregs cell function is IL-10, which inhibits the production of pro-inflammatory cytokines and supports regulatory T cell differentiation. However, the effect of MSCs on B cell is still poorly understood [80].

The therapeutic efficacy of MSCs in CVDs depends mainly on their paracrine activity. Besides their immunomodulatory action, MSCs secrete dozens of active biological factors that exert profound effects on local cellular dynamics [81]. The formation of new vessels after ischaemia is the basis of tissue repair [82] and MSCs may promote would healing mainly by participating in enhancing angiogenesis through the release of Vascular Endothelial Growth Factor (VEGF).
Moreover, necrotic myocardial cells in the infarcted area are replaced with fibroblasts leading to ventricular remodeling, arrhythmias or even death. In this context, MSCs can regulate matrix metalloproteinase to inhibit fibroblasts activation (in myofibroblasts), reduce ECM deposition, reduce LV remodeling and ultimately improve myocardial function. Matrix metalloproteinases (MMPs) in the myocardium, secreted by myofibroblasts, are the driving force behind myocardial matrix remodeling. The expression of MMPs is generally found at low levels in normal adult tissue but is upregulated during certain pathological remodeling processes. They are stimulated by a variety of inflammatory cytokines and growth factors such as IL-6, tumor necrosis factor-α (TNF-α), Epidermal Growth Factor (EGF), Platelet-Derived Growth Factor (PDGF) and are inhibited by

a group of endogenous proteins, namely Tissue Inhibitors of Metalloproteinases (TIMPs). In this context, when exposed to pro-inflammatory cytokines and hypoxia, MSCs counter these stresses by inhibiting MMPs *via* secreted TIMPs [83],[84]. Additionally, several studies have shown that HGF secreted by MSCs is an inhibitor of fibrosis and that HGF is the primary component responsible for ant-fibrotic effect of MSCs *in vitro* [3]. Further, MSCs release Granulocyte Colony-Stimulating Factor (G-CSF), a strong bone marrow stem cells mobilizer. Several studies have shown that Bone-Marrow Mesenchymal Stem Cells (BM-MSCs), mobilized by G-CSF promote the repair of various damaged tissue types, including the myocardium. Further, Stromal cell-Derived Factor-1 (SDF-1) secreted by MSCs play an important role in stem cells mobilization, chemotaxis, homing and colonization of damaged myocardial tissue post MI event [48], [81],[85],[86], [87],[88]. Finally, MSCs have been shown to possess a low immunogenic potential. These effects make them a promising tool in the treatment of Myocardial Infarction [80].

Currently, the MSCs most commonly used in clinical studies are mainly derived from bone marrow and adipose tissue. However, the techniques used to isolate bone marrow-derived stem cells are considered invasive and painful and are associated with potential donor site morbidity and high risk of contamination. Adipose-Derived Stem Cells (ADSCs) are considered more advantageous than bone marrow-derived stem cells because they are easily cultured, easily expanded, and repeatedly obtained from fat tissue collected by patients undergoing liposuction. The number of collectable ADSCs per volume is higher than other types, e.g., in comparison with the same volume of bone marrow. In fact, the number of ADSCs obtained from 1g of fat ($5x10^3$ cells) is approximately 500-fold greater than the number of mesenchymal stem cells isolated from 1g of bone marrow. ADSCs also have an increased proliferative ability compared to bone marrow-derived stem cells. Additionally, the number of ADSCs does not decrease with age, and they are less senescent than bone marrow-derived stem cells. Furthermore, ADSCs are equivalent to -if not better than- bone marrow-derived stem cells in terms of differentiation potential and

immunomodulatory effects [89],[90]. For these reasons, ADSCs are a potential therapeutic instrument for many diseases, including MI [91],[92].

In context of MI, ADSCs are suitable since they have a significant potential for angiogenesis and vasculogenesis. Additionally, they secrete several cytokines and growth factors with anti-apoptotic effect, anti-inflammatory activity and capable to promote the recruitment of other stem cells to the myocardium after ischaemic injury [93]. However, large numbers of cells are required to obtain a sufficient number of cells for their clinical applications. Thus, the *in vitro* expansion has to be scaled up considerably in order to generate a sufficient quantity of cells for treating cardiac ischaemia [94].

To date, there have been several human clinical trials of ADSCs for ischaemic heart disease. The APOLLO trial was designed to assess the safety and feasibility of intracoronary infusion of ADSCs in the treatment of patients in the acute phase of MI. Fourteen patients were enrolled to receive an intracoronary infusion of 20 million of ADSCs in the culprit artery. The main findings of APOLLO trial were **1)** liposuction to harvest ADSCs in the acute phase of an AMI is safe and feasible; **2)** intracoronary infusion of freshly isolated ADSCs was safe and did not result in an alteration of coronary flow or any indication of microvascular obstruction; **3)** no unanticipated adverse effects related to ADSCs-based therapy were reported. Finally, **4)** ADSCs injection resulted in a trend toward improved cardiac function, accompanied by a significant improvement of the perfusion defect and a 50% reduction of myocardial scar formation [95]. Moreover, the PRECISE trial was designed to examine the safety and feasibility of delivering ADSCs by transendocardial route in 36 patients with advance coronary artery disease not amenable to any revascularization procedures. The results demonstrated that obtaining autologous ADSCs *via* liposuction and delivering them by transendocardial injection, they are safe and feasible in patients with ischaemic cardiomyopathy [96].

1.8. Stem cell-based therapy clinical challenges

More than a thousand clinical trials investigate the MSCs for several clinical applications, including cardiac disorders. However, the therapeutic functions of MSCs administered to humans are not as robust as demonstrated in pre-clinical studies. Indeed, the translation of stem cell-based therapy is impaired by many limitations such as the diverse origin of MSCs, the challenges associated with administration of MSCs, the challenges of the host environment and the difficult in predicting immunomodulatory and regenerative effects that can lead to unpredictable therapeutic outcomes [49].

Local administration of MSCs is commonly used in clinical indications as it provides direct access to the disease site that often results in better therapeutic response [97]. However, insufficient retention and survival of transplanted MSCs at the site of injury associated with local administration are not still addressed. The retention is defined as the duration of localization of the cells at the target site. The lack of retention following local administration has been attributed to multiple issues including cell death due to the hostile environment encountered at the disease site and the poor engraftment into the tissue [49]. Accordingly, in a study using intracoronary injection of bone marrow stem cells in patients with MI, only 2.1% of radiolabeled stem cells remained at the site of injection after 1 hour. In addition, most of the remaining signal was found primarily in the liver and spleen [98]. Furthermore, the cells at the target site are often no longer viable due to immune-mediated damage and apoptosis [99]. The nonviable cells have a reduced capacity to produce therapeutic factors, which can compromise the efficacy of the MSCs therapy. Thus, despite the local delivery of paracrine factors directly to the injured area following local administration of MSCs represents an important advantage of this path, it is not a feasible option up to now.

Alternatively, intravenous injection of MSCs is used, but the therapeutic utility has been limited due to insufficient homing to the target site. Furthermore, an insufficient residence time at the target site occurred. Indeed, when MSCs are delivered systemically, a key factor for exerting maximal therapeutic benefit is their ability to remain in circulation for long enough to deliver therapeutic payloads to the damaged tissue. However, intravenously administered MSCs are immediately concentrated in the lung capillaries and phagocytosed by monocytes within 24 hours [100]. This limits the ability of MSCs to deliver therapeutic payloads at the site of injury, *via* secreted paracrine factors, to a short period and limits cell homing to target tissue. Entrapment of MSCs in the lung capillaries also increases susceptibility to immune clearance [101]. All these evidences pushed the researchers to find new strategies to improve MSCs administration.

1.9. Bioengineering approaches for improving MSC administration

To improve local MSCs administration, multiple strategies have been investigated. Recently, biomaterials have gained great interest to overcome the bottlenecks regarding stem cell-based therapy [102]. Naturally derived polymeric materials, including polypeptides (e.g., collagen) and polysaccharides (e.g., hyaluronic acid) have been explored extensively as scaffolding materials [103],[104]. Collagen is the main structural protein of most hard and soft tissues in human body, which plays an important role in maintaining the biological and structural integrity of the ECM and provides physical support to tissues. Collagen can be extracted and purified from a variety of sources and offers low immunogenicity, a porous structure, good permeability, biocompatibility and biodegradability and has functions to regulate the morphology, adhesion, migration and differentiation of the cells [105],[106],[107]. Hence, collagen scaffolds have been widely used in tissue engineering due to these excellent properties. However, the poor mechanical property of

the collagen scaffolds limits their applications to some extent [108]. In addition to the generally weak mechanical strength, naturally derived polymers are typically enzymatically degradable and their kinetics of degradation is not easily controlled or predicted [109]. On the other side, synthetic polymers can be reproducibly manufactured with a wide range of mechanical properties and degradation kinetics [110]. Among others, scaffolds comprising poly(lactic-co-glycolic acid) (PLGA) have been vastly investigated for tissue regeneration. Unfortunately, synthetic polymers do not facilitate cell attachment as a natural polymer would. For this reason, coating of synthetic polymeric scaffolds with naturally derived polymers (collagen or gelatin) and ceramics (calcium phosphate) for tissue engineering applications have been explored [111]. The success of a scaffold technology in modulating the microenvironment in the implantation site depends largely on the action of the cells present on the substrates or infiltrating to the site of injury [109]. Thus, MSCs encapsulating-biomaterial providing a mechanical barrier that helps both placement cells at the target site and protect them from immune system assault. Specifically, alginate hydrogel increased MSC retention in healed MI and facilitated paracrine effects such as increased microvasculature and decreased scar formation [112]. However, the bulk size of hydrogel is only suitable for local MSCs administration, not for systemic administration. Microgels encapsulating MSCs is another bioengineering solution to enhance the residence time and survival of MSCs. Unlike bulk hydrogel, which is only suitable for local administration, microgels can be suitable for both local and systemic injections. One potential limitation is that the physical barrier of the microgel may mask the receptors on the MSCs surface that are important for their homing to injured sites, although this may be addressed by using additional homing ligands on the microgel [49]. Indeed, to improve the homing of MSCs to the target sites, the surface of MSCs can be modified with different homing ligands, by improving the interaction between MSCs and the inflamed damaged tissue. This can be achieved through genetic engineering, antibody conjugation, or polymer coating of MSCs. Besides, MSCs can be engineered with intracellular iron oxide to efficiently direct MSCs to reach the target sites under guidance by

an external magnetic field. Additionally, iron oxide makes it possible to monitor the biodistribution of MSCs using magnetic resonance imaging.

These bioengineering strategies may help to improve clinical outcomes for various diseases by addressing the challenges of insufficient MSC residence time and homing to diseased sites but more work is required to achieve a critical mass of MSCs at the target site that can predictably modulate the biological signaling pathways [49].

It is also been demonstrated the correlation between the host immune response and the efficacy of MSCs therapy [113]. Indeed, the immunosuppressive efficacy *in vivo* of administered MSCs is related to the recipient response against the infused MSCs. Thus, the host immune responses play an important role in mediating the therapeutic benefit provided by cell-based therapies. Accordingly, to this, the outcomes of MSC activation might vary depending on the levels and the type of inflammation within the residing tissues [114]. Additionally, previous studies on environmental hypoxia have indicated that exposing MSCs to hypoxic condition can induce various soluble bioactive molecules and enhance their angiogenic and regenerative potential [115]. This awareness that the role of the host environment in MSC function helped to address novel approaches for MSC engineering (such as priming MSCs with inflammatory cytokines) represents an interesting bioengineering approach to boost their potency toward therapeutic applications [49].

Stem cell spheroids, which are 3D spherical cellular assemblies, have recently garnered much attention as promising avenues for stem cell-based therapy [116],[117]. Accumulating evidences have suggested that three dimensional (3D) culture systems (e.g. spheroids) offer a cellular niche that is more similar to the microenvironment of native heart tissue compared to two dimensional (2D) culture systems [15]. Spheroid formation enables the cells to assemble and interact under native forces and allows them to generate their own ECM. When the cells contact, interact and communicate with other cells, rather than with the scaffolds, the cell culture more closely

replicates the *in vivo* environment. Therefore, spheroid culture may be an efficient method to maintain the potentialities of MSCs. However, several barriers exist in the *in vivo* translation of spheroid-based stem cells therapy. For example, the controlled differentiation of stem cell spheroids into specific cell lineages. Besides, restricted diffusion of oxygen, nutrients, and growth factors into the core of spheroids can often induce cell apoptosis during long-term culture *in vitro*, a phenomenon known as necrotic core [118].

1.10. Aims of the project

Although strategies such as the use of biomaterials can help address these challenges, most studies have not solved the issues related to cell survival and engraftment *in vivo,* yet. Recently, our group fabricated an implantable flexible device for loco-regional sustained drug delivery: the microMESH. The microMESH is designed for the long-term release of multiple therapeutic molecules. It can perfectly adhere with the tissues in the implantation site due to its peculiar flexibility, which allows a more targeting pharmacological therapy. The microMESH is fabricated employing a top-down fabrication approach, returning a device with a precise geometry and physico-chemical features. Made of biocompatible, biodegradable and FDA-approved polymers for clinical applications, microMESH, with its tiny size proved effective benefits in the treatment of glioblastoma multiform. In malignant gliomas, microMESH ably wrapped around the brain tumor crating a closer interaction with the tumor mass, increasing the therapeutic efficacy of the device [119]. The aim of my Ph.D. research program was to test the effect of microMESH, fabricated in three different geometries, on the interaction and consequently biological activity of a Mesenchymal Stem Cells line, namely human Adipose-Derived Stem Cells hADSCs for the therapeutic application in Myocardial Infarction (MI). To address these goals, I firstly manufactured microMESH in three different geometrical features. Later, I deeply investigated the

effects of the microMESH geometry on hADSCs biological behavior evaluating: 1) how they interact with the substrates; 2) how the cell cytoskeleton changed on microMESH; 3) the safety of these substrates, comparing the cell viability at 24h, 48 and 72h; 4) the secretome of hADSCs on microMESH exposed to TNF-α stimulation in order to shed new light on the ability of geometry microMESH to play a role in modulating the cell response to environmental stimuli and 5) the hADSCs stemness on microMESH to investigate if the geometry might influence this process.

Chapter 2

2.1. Abstract

The deposition of cells at sites of injury is a clinically relevant approach to facilitate local tissue regeneration and repair. However, cell engraftment, retention, and survival are generally modest, requiring the development of novel deposition techniques and biomaterials. Here, a micro-sized polymeric network (microMESH) is investigated as a promising biodegradable scaffold for the engraftment and tissue integration of human Adipose-Derived Stem Cells (hADSCs) to be used for a wide range of injuries, including myocardial infarction. microMESH comprises a regular network of PLGA microfilaments spatially organized to form square openings of 5x5, 10x10 and 20x20 μm^2 . microMESH is realized using soft lithographic techniques starting from a master silicon template reproducing the actual geometry of the final PLGA network. After extensive geometrical, physico-chemical, and mechanical characterizations using a broad range of techniques, hADSCs were integrated with microMESH. Cell viability, spatial organization, secretome and stemness were characterized for all three different microMESH configurations and compared to conventional systems, including 2D plastic dishes and collagen layers. Interestingly, when hADSCs were cultured on microMESH they organized in spheroidal-like structures, despite the geometry, maintaining viability over time. This peculiar attitude of the microMESH to form assemblies better represents the human tissue outside the body, compared to 2D monolayer cultures. Additionally, spheroids established an intimate interaction with the microMESH resulting in the scaffold incorporation within the 3D arrangement formed by the cells. On the contrary, hADSCs form only superficial interaction above the flat collagen sheet that is currently used for cell transplantation in animal models of cardiac diseases. Moreover, once the hADSCs are placed on microMESH, the actin cytoskeleton reorganizes to confer a 3D cell shape with multidirectional actin arrangements, forming nonlinear structures and ring structures at the anchorage site to the

microMESH, relative to linear filaments when the cells adhered and flattened onto the plastic surface and on top of collagen scaffold. This internal reorganization and the stronger interaction may explain why microMESH scaffold fostered the secretion of biologically active molecules, acting in a paracrine fashion on resident cells, which are expected to accelerate tissue regeneration and repair. Specifically, when hADSCs grew on microMESH we observed a trend for higher production of several factors with specific implications in angiogenesis, stem cell proliferation and expansion, cell survival, inflammation modulation, ECM remodeling, stem cell mobilization, chemotaxis and homing, relative to 2D monolayer conditions. The paracrine effect of hADSCs is scaffold dependent and can be modulated by tailoring the geometrical and mechanical properties of microMESH. Indeed, the 5x5 microMESH showed its contribution in angiogenesis, ECM remodeling and stem cell mobilization from bone marrow into the bloodstream. Indeed, highest amounts of VEGF, TIMP-2 and GCSF, respectively were detected in 5x5 geometry compared to the other conditions. Rather, 10x10 geometry promotes angiogenesis enhancing the VEGF production, stem cell proliferation and survival by raising the Fibroblast Growth Factors family secretion and EGF factor, respectively and favors ECM remodeling increasing the TIMP-2 production compared to other conditions. Lastly, the 20x20 seems to have a more anti-inflammatory role (combination of IL-10 and TGF-β1) and chemotactic function (e.g. RANTES). Finally, in this work, we started to shed new light on the ability of micromMESH geometry to modulate the hADSCs stemness evaluating the expression levels of CD44, CD90 and CD105 markers over time. The proposed microMESH scaffold is expected to provide an effective alternative to more conventional hADSCs transplant techniques.

2.2. Introduction

Cardiovascular disorders remain the major cause of morbidity and mortality across the world and over the last decades, death rates have increased significantly [120]. The regenerative capacity of adult human heart is limited and grossly inadequate to compensate the severe loss of cardiomyocytes occurring after Myocardial Infarction [1],[121]. MI can ultimately develop into heart failure, for which heart transplantation is the only curative therapy [122]. Despite the positive outcomes in heart transplantation, there is a severe organ shortage worldwide, and the number of organs available does not meet the demand [122]. Additionally, drugs can only delay the progression of heart disease. In fact, they can not save the function of infarcted CMs. Therefore, alternative strategies are necessary. Stem cell-based cardiovascular tissue regeneration therapy might be indicated as a promising alternative for MI treatment [123],[124]. Initial animal studies using adult stem cells reported improved heart function through the formation of new cardiomyocytes by transdifferentiation of the injected cells [31]. However, adult stem cell transdifferentiation was not observed in later studies [125],[126] and the ability of Mesenchymal Stem Cells (MSCs) to regulate the immune response through a paracrine activity was discovered. Indeed, MSCs are an excellent candidate for cell-based therapy due to their paracrine activity by which cytokines and growth factors released by the transplanted cells directly regulate tissue repair and regeneration with specific involvement in vascularization, anti-fibrotic effect, cell survival, immune system regulation, Extra Cellular Matrix remodeling and stem cell homing [127]. Adipose tissue is a suitable MSCs source. Adipose-Derived Stem Cells (hADSCs), a MSCs line, presents several advantages, such as easy culture, abundance and easy isolation process from fat tissue collected by patients undergoing liposuction. Additionally, it presents immunomodulatory propriety and pro-angiogenic and anti-inflammatory effects [128].

However, a significant barrier in MSC therapy concerns the inability to implant these cells to the diseased site with high efficiency and good engraftment [129]. Biomaterials can serve as a

promising platform to overcome such limitations and improving cell engraftment and survival *in vivo* [130]. Different biomaterials have been tested to support stem cells implantation to the heart, including collagen [131]. Collagen, the most abundant component of the heart, in addition to its biocompatibility and biodegradability, has low immunogenicity proprieties and allow the cells, grown on top of it, to adhere homogenously to its surface, forming a 2D monolayer. Nevertheless, several studies showed that the microenvironment of native heart tissue might be better replicated when stem cells are cultured in 3D structures, compared to 2D monolayer culture [15],[132].

Here, we propose a novel polymeric micro-sized scaffold, the microMESH, in three different geometries and our studies relatives to the effects of combining these scaffolds with hADSCs, to determine microMESH potential as cell-carrier sheet for future therapeutic application in MI.

To address this goal we primarily fabricated three types of microMESH differing in terms of squared holes size in its structure. Secondarily, we investigated the influence of microMESH geometry on the biological behavior of hADSCs performing different studies such as cell interaction with microMESH, cell viability, cell cytoskeleton organization, secretome and stemness comparing the outcomes with a flat collagen substrate, a without-holes scaffold.

2.3. Materials and methods

Materials: Polydimethylsiloxane (PDMS) (Sylgard 184) was purchased from Dow Corning (Midland, Michigan, USA). Poly-(vinyl alcohol) (PVA), poly-(lactic-co-glycolic) acid (PLGA) (50:50), Rhodamine B (RhB) and Acetonitrile (ACN) were obtained from Sigma Aldrich (Saint Louis, Missouri, USA). Curcumin (CURC) was acquired from Alfa Aesar (Haverhill, Massachusetts, USA). Collagen Cell Carrier (CCC 10x10, geklebter Rand) was obtained from Viscofan Bioengineering (Weinheim, Germany). High-glucose Dulbecco's modified Eagle's Minimal Essential Medium (DMEM), heat-inactivated fetal bovine serum (FBS), Penicillin, Streptomycin, L-Glutamine solution, Dulbecco's Phosphate Buffered Saline (PBS), Trypsin-EDTA solution, Paraformaldehyde (PFA), and Tumor Necrosis Factor-α (TNF-α) were acquired from Sigma Aldrich (Saint Louis, Missouri, USA). Human Recombinant Basic Fibroblast Growth Factor (bFGF) was gained from Merck (Darmstadt, Germany) whereas Typan Blue Stain (0,4%) from GIBCO (Invitrogen Corporation, Giuliano Milanese, Milan, Italy). 2'-[4-ethoxyphenyl]-5-[4-methyl-1-piperazinyl]-2,5'-bi-1H-benzimidazole trihydrochloride trihydrate (Hoechst 33342) and Bovine Serum Albumin Standard Ampules, 2 mg/mL derived from Thermo Fischer (Waltham, Massachusetts, USA). Bicinchoninic Protein Assay kit (BCA) was obtained from Euroclone (Pero, Milan, Italy). Cytokine Array-Human Cytokine Antibody Array (Membrane, 80 targets), PE anti-CD44 antibody, FITC anti-90/Thyl antibody and APC Anti-CD105 antibody were acquired from Abcam (Cambridge, UK). FITC Annexin V/Dead Cell Apoptosis kit, Alexa Fluor 488 Phalloidin were sourced from Invitrogen (Waltham, Massachusetts, USA).

Fabrication of the microMESH

A top-down fabrication approach was employed to realize a polymeric micromesh (microMESH) in three different geometries, namely 5x5, 10x10 and 20x20. Both, 5x5 and 10x10 microMESH are defined by orthogonal strands (5μm) evenly spaced by 5 and 10μm squared holes respectively; whereas, 20x20 microMESH presents 20x20 μm^2 openings divided by 3μm wide strands. In all the three configurations, microMESH strands are 5μm thick.

The top-down fabrication technique involves multiple sequential steps. The first step is the fabrication of a silicon master template via Direct Laser Writing (DLW), which enables to transfer the specific arrays of pillars required for the final microMESH geometry on the silicon wafer. Then, a PDMS solution is deposited over the silicon template. After 4h of polymerization at 60°C, the PDMS template, presenting the negative geometry of the silicon one, is replicated into a PVA template by pouring a PVA solution (3,5 % w/w in water) on top of it. After one hour and a half at 60 °C, the polymerized PVA template displayed the same arrays of pillars as the original silicon template. Then, a polymeric paste of PLGA is uniformly dispersed to fill up accurately the ridges between the micropillars over the PVA template. The three geometries required different loading amount of PLGA, because of the different microMESH volume per geometry for the same template size. Specifically, the amount of PLGA needed to load completely all the grooves in the 5x5, 10x10 and 20x20 PVA layers was 24.5, 18.2 and 5mg, respectively. In all cases, PLGA was dissolved in Acetonitrile (ACN) and spread overall surface of the whole PVA template. Following the solvent evaporation, the final microMESH is released by dissolution of the PVA supporting component in water. The strands and holes of the PLGA meshes reproduced the geometries of the corresponding PDMS templates (**Figure 5**).

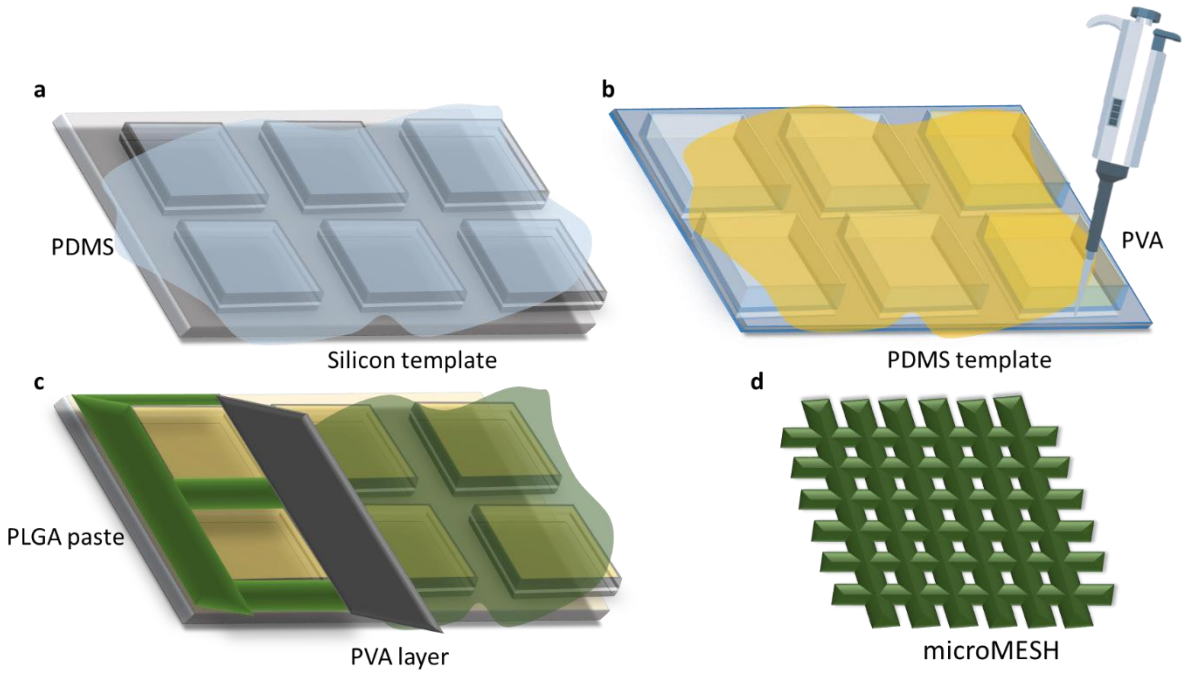

Figure 5. Multistep procedures for microMESH realization. The top-down fabrication strategy involves different sequential steps. **a)** The first step is the fabrication of a silicon master template via Direct Laser Writing (in grey). Then, a PDMS solution (in light blue) is deposited on top of the silicon template. **b)** The PDMS template is replicated into PVA template by pouring a PVA solution (in yellow) on top of it. Later, **c)** the polymerized PVA template with the same arrays of pillars as the original silicon template is loaded with a polymeric paste of PLGA (in green) to fill up the empty wide strands between the micropillars over the PVA template. PLGA is dissolved in Acetonitrile and spread overall the surface of the PVA template using a blade. Finally, **d)** following ACN evaporation, the final microMESH is released by full dissolution of the PVA component in water.

microMESH characterization

Scanning Electron Microscopy (SEM, JSM 6490, JEOL, Milan, Italy) was used to image the microMESH in each geometry. After PVA dissolution in water, a piece of PLGA net was placed on a silicon template and uniformly sputter–coated with 10nm of gold to increase the contrast and reduce sample damaging. An acceleration voltage of 10kV was employed for SEM imaging.

Additionally, confocal microscopy (Nikon A1, Dexter, MI) was used to study the structure of all the microMESH types as well as the uniform distribution of its loading. To this end, curcumin (CURC) for its intrinsic fluorescence was mixed with PLGA and dissolved in ACN. Then, the resulted polymeric paste was spread on top of the PVA template.

hADSCs interaction with the substrates

Human Adipose-derived Stem Cells were used to perform all the *in vitro* experiments. Cells were provided by the University of Navarra, Spain (Laboratory of Cell Therapy, Division of Cancer, Foundation for Applied Medical Research) and cultured at 37°C in 5% CO_2, in high-glucose DMEM, supplemented with 10%FBS, 1%Penicillin-Streptavicin, 1%L-Glutamine and bFGF (1 ng/mL), from now on named culture medium. Per each geometry, $5x10^5$ cells were seeded on top of two squares of microMESH, still supported by a PVA layer, located apart from each other, placed on the bottom of a Petri dish. Each microMESH size was $2.5x2.5cm^2$, derived by precisely cutting the initial $4x4cm^2$ template with a surgical scalpel. The cells were carefully positioned in separate drops and homogeneously distributed all over the surface of the microMESH (**Figure 6a**). Few minutes later, the culture medium wetted the entire surface of the substrates (**Figure 6b**) and the PVA component started to dissolve, releasing the final microMESH with its peculiar shape of a micrometric polymeric net made of regular openings, which are also micrometric, capable to interact with the cells. After 8h from seeding, to allow the cells to interact with the substrates, the scaffolds were covered with the culture medium to prevent the dehydration of the cells throughout the analysis. Due to the microMESH holes, cells could pass through its openings, falling down and adhere to the bottom of the plate. Therefore, the scaffolds were relocated in another Petri dish already containing fresh culture medium, which made it easier the proper adaptation of the scaffolds in the new plate, removing the cells not tightly attached to the microMESH, thus ignoring their contribution over the results (**Figure 6c**). The interaction of

hADSCs with the microMESH was examined in comparison to a regular plastic dish (2D Petri dish) and a collagen scaffold (2D collagen) made of pure collagen type I fibers. For the analysis, cell nuclei were stained with Hoechst 33342 to better recognize cells aggregates distributed in 3D spheroidal-like structures on top of the PLGA meshes. The physical features of these structures were investigated using a fluorescent microscopy (Leica 6000, Wetzlar, Germany) at different time points, namely 24, 48 and 72h, acquiring images of the entire µMESH substrates. The analysis resulted in a collection of images. After that, ImageJ was used to analyze and characterize each spheroid present in these images, in terms of number of spheroids per microMESH, perimeter (in µm) and aspect ratio. Thanks to the fluorescence of spheroids-forming cell nuclei, it was possible to calculate precisely the perimeter, as the length of the outside boundary of the spheroid examined, and the aspect ratio, as the ratio between the major axis and the minor axis of the same object.

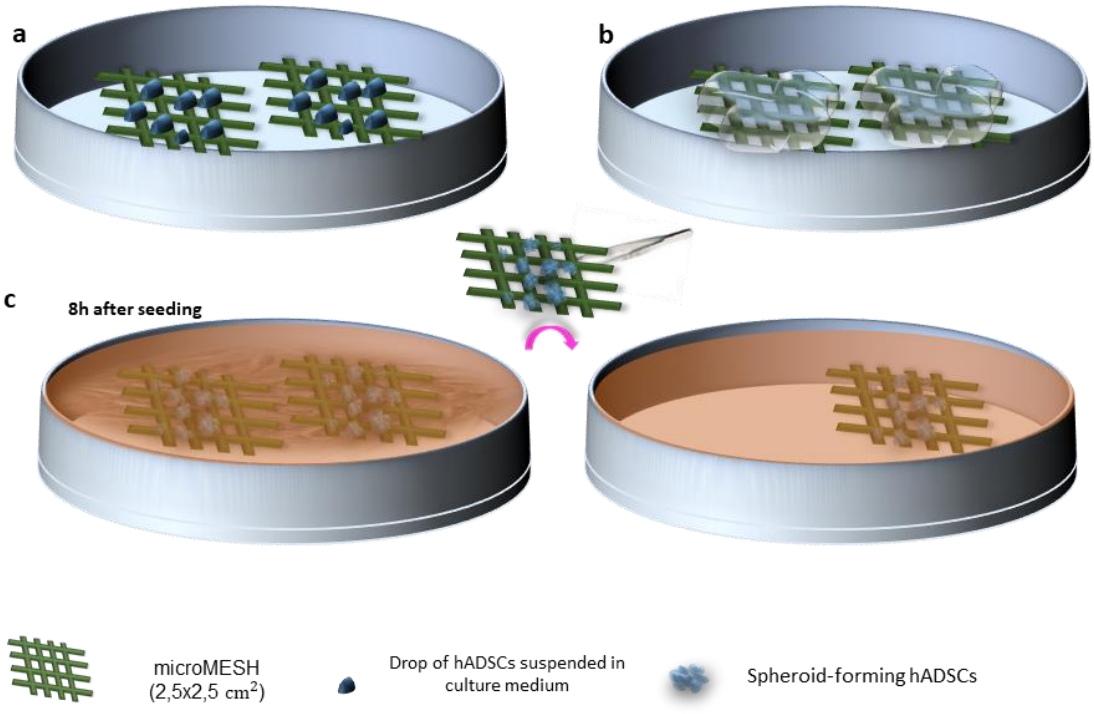

Figure 6. Schematic of the experimental design to study the interaction between hADSCs and the microMESH. **a)** Placement of the microMESH on the bottom of a plastic dish and cell seeding in separate drops. **b)** Partial dissolution

of the PVA backing layer and release of the final microMESH. **c)** Relocation of the microMESH in another Petri dish in order to remove cells not firmly attached to the scaffolds.

Single cell suspension from hADSCs spheroids on microMESH

As in the present work cells were seeded and grow on top of different scaffolds, forming monolayers or spheroids, it was important to find a suitable protocol for their detachment from these substrates and dissociation into single cells, prior the subsequent flow cytometry analyses. The cells were initially seeded on top of a plastic dish, flat collagen sheet, 5x5, 10x10 and 20x20 microMESH, as mentioned before, in drops and suspended in culture medium. Then, to dissociate the spheroids anchored on top of any geometry of microMESH, 24, 48 and 72h after seeding, according to the time point considered, the scaffolds were moved to another plastic dish and the cells not tightly anchored to the substrates were discarded (**Figure 7a**). After a wash with PBS, the cells were incubated with Trypsin-EDTA solution for 10 minutes (**Figure 7b**). Here, the spheroids formed resulted detached from the micrometric nets, but only partially dissociated into single cells. The dissociation was further promoted by gently pipetting up and down avoiding any cell damage, for 5 min, resulting in the full disaggregation of the spheroids into single cells. A similar procedure was used for cell detachment from the collagen scaffold. Briefly, 24, 48 and 72h after seeding the collagen scaffold was relocated and the formed cell monolayer was firstly washed with PBS and later, incubated with trypsin for 10 min. After the incubation period, a single cell suspension was obtaining by pipetting less vigorously than the previous conditions. The dissociation process was carefully monitored by microscopic analysis. Then, the individual cell suspension of each condition was collected in PBS and filtered using 40µm cell strainers. Finally, the single cell suspensions were centrifuged for 6 min at 200 x g, resuspended in culture medium and counted using an automated cell counter (ChemiDoc MP, BIORAD) (**Figure 7c**).

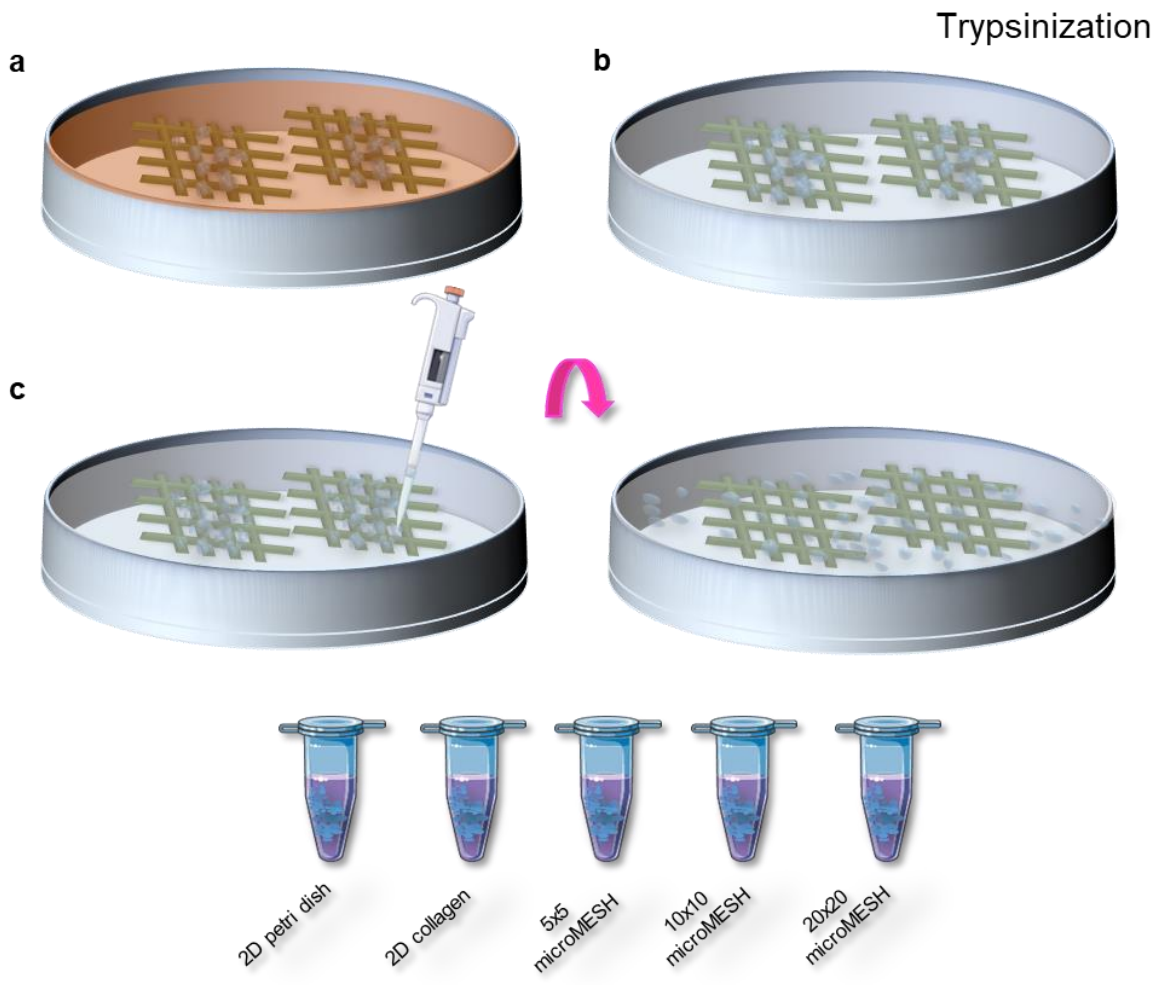

Figure 7. Overview of the spheroids disaggregation protocol. The schematics show the step-by-step procedure including **a)** hADSCs seeding and their aggregation into spheroids over the microMESH. **b)** Incubation with trypsin and finally, in **c)** spheroids dissociation into single cells, which are later collected in small tubes suspended in culture medium.

hADSCs viability study

The viability of hADSCs was determined using an Annexin V-FITC Apoptosis Detection Kit and flow cytometry. To perform this experiment, after a wash with PBS the individual cell suspensions, obtained as just described above, were centrifuged and resuspended in 1X Annexin Binding Buffer prepared by adding 1mL of 5X Annexin Binding Buffer, provided by the kit, to 4mL

deionized water. One million of cells were diluted in 1mL of 1X Annexin Binding Buffer. The single cell suspensions were incubated for 15 min at RT, protected from light, with 1.25µL of Annexin V-FITC and Propidium Iodide (PI, at 100µg/mL). The working solution of PI was prepared by dilution of 1 mg/mL PI stock solution in 45µL of 1X Annexin Binding Buffer. Specifically, 1µL of 100µg/mL PI working solution was added to each 100µL of cell suspension ($1x10^5$ cells). After the incubation period, 400µl of 1X Annexin Binding Buffer was added to each sample, which were immediately stored in ice and vortexed right before the analysis. Flow cytometry was performed using a FACS ARIA (Becton Dickinson, Franklin Lakes, NJ, USA) and the data were analyzed using FACSDiva 9.0.1 software. The experiments were performed independently at least four times.

hADSCs cytoskeleton organization study

Cells were stained with Hoechst 33342 before seeding in order to avoid the dye accumulation over the scaffolds and red fluorescent molecule Rhodamine B (RhB) was incorporated in the PLGA polymeric paste and spread on top of the three PVA layers. Briefly, to prepare RhB-loaded microMESH, 2µL of an RhB solution (2mg/mL in ACN) was added to the PLGA paste before spreading it on top of the PVA template of the geometry corresponding. The resulting microMESH, still having the PVA reinforcement were cutted in pieces of $1cm^2$ size and placed on the bottom of an 8 well plate. Similarly, a square piece of collagen was positioned in a well. A cell suspension, at a density of $1x10^4$, were seeded on top of each scaffold for 24h. After this period, the cells were repeatedly washed with cold PBS (3x5 min) and fixed with 0.4% paraformaldehyde (PFA) at Room Temperature (RT) for 1h. Then, the cells were washed again with PBS (3x5 min) and permealized using 0,1% Tryton X-100 in PBS for 20 min. Later, the cells were stained with 5µL of Phalloidin-488, which binds to cell actin, in PBS supplemented with 1% Bovine Serum Albumin (BSA) and 0.01% Tryton X-100 for 1h. Confocal images were used to calculate the percentages of nonlinear and linear actin within the cells cultured in all the scaffolds tested. ImageJ was used

to analyze each image. Images were primarily binarized, then auto-thresholded. A threshold was made using the 'Default' threshold method. Thresholded images were set in terms of size (0-infinity) and circularity (0-1) resulting in a collection of actin objects. Finally, the objects with an aspect ratio major than 5 were classified as linear, while an aspect ratio minor than 5 was considered as nonlinear actin fiber.

hADSCs secretome analysis under pro-inflammatory insult

The main therapeutic effect of hADSCs is due to their paracrine action. Accordingly, the secretomes of hADSCs cultured in all the five conditions mentioned were analyzed. The study was performed in a model of inflamed microenvironment, whereby TNF-α, a pro-inflammatory cytokine, was added to the medium to mimic the inflammatory milieu existing in the post-MI heart, in order to shed new light on the ability of the geometry microMESH to influence the paracrine activity of hADSCs in responding to the surrounding microenvironment. To perform this experiment, the cells were cultured in controlled environmental conditions (37°C in 5% CO_2) suspended in culture medium and seeded ($5x10^5$ cells) on top of the different substrates, and at the same density on a plastic dish. After the incubation period (8h), all the scaffolds were moved to a new Petri plate, with the corresponding condition, already containing 10 mL of DMEM supplemented with 2% FBS, 1% L-Glutamine, 1%Penicillum-Streptavicin and TNF-α [10 ng/mL], from now on named pro-inflammatory culture medium. Similarly, 8h after seeding the 2D condition culture medium was replaced with pro-inflammatory culture medium. Cells supernatants were collected 48h after seeding, and the cytokines, chemokines and growth factors released by the cells were analyzed by a cytokine antibody array according to the manufacturer's instructions. The cytokine arrays are an antibody-pair-based assay that use a membrane as a substrate. Capture antibodies are supplied spotted on a membrane with each spot capable to detect a different cytokine. The array used assessed contemporarily 80 different factors. Briefly, the

supernatants were previously quantified in terms of total protein by BCA assay, to use the same amount of proteins in every condition. Later, the supernatants were added to the membranes and kept overnight at 4°C (incubation period). The day after, following several washes with Wash Buffer I and Wash Buffer II, provided by the kit, biotin-conjugated anti-cytokines antibody was added to each membrane at RT for 2h. Afterwards, it was made the incubation with HRP-Conjugated Streptavidin at RT (2h). Finally, the membranes were analyzed using the chemiluminescent method (ChemiDoc MP Imaging System by Bio-Rad) and by using ImageJ, the luminescence associated with each spot was quantified, with higher value assessing a higher amount of that factor included in the sample. A baseline, considered as the average value obtained from the negative control spots, was subtracted to all the 80 values and finally, all the obtained values were normalized by the average value of the positive control spots. In this way, it was possible to compare the data related to the cells cultured in all conditions.

hADSCs phenotypic characterization on microMESH

The single cell suspensions were obtained using the protocol for spheroids disaggregation we developed. Spheroids-derived hADSCs were incubated with PE Anti-CD44 antibody, FITC Anti-CD90 antibody and APC Anti-CD105 antibody for 1h at room temperature protected from light. After the incubation period, the cells were washed by centrifugation at 200g for 6 min and resuspended in 500µL of PBS. Finally, the samples were kept in ice until the analysis.

Statistics analysis

The statistical analyses were performed using Graph Pad Prism 8.0. The values are presented as mean ± standard deviation (SD). Each experiment was repeated multiple times independently

(at least ≥3). The statistically significant differences between groups were evaluated with ordinary one-way ANOVA test with Tukey's Multiple Comparison Test as post-hoc test.

2.4 Results

Manufacturing and characterization of microMESH

A top-down fabrication strategy was employed to realize three different microMESH configurations, namely 5x5, 10x10 and 20x20 in which peculiar geometrical features are transferred from a silicon master template to a PVA layer, passing through an intermediate PDMS template. Both the original silicon template and the PVA layer present a regular pattern of 5x5, 10x10 and 20x20 μm^2 micropillars, according to the geometry considered as it is possible to observe in **Figure 8a** (upper panel). PVA pillars, in all configurations has a thickness of 5μm. Following full dissolution of the PVA supporting layer in water, a solid PLGA mesh is released. The final microMESH is a net made of polymeric strands (5μm wide for the 5x5 and 10x10 microMESH and 3μm wide for the 20x20 geometry) separated by openings of 5x5, 10x10 and 20x20 μm^2, which precisely reflect the geometry of the micropillars in the initial silicon template (**Figure 8b,** middle panel). The empty spaces in their structure make the three polymeric PLGA networks designed very flexibles thereby they could adhere with the tissues in the implantation site, a key feature for tissues regeneration and repair. The fluorescent microscopy images in **Figure 8c** (bottom panel) show a continuous green signal, associated with CURC-loaded PLGA strands. These images document the regular structure of the polymeric mesh as well as the uniform distribution of its payload. Altogether, the data suggest that the top-down fabrication approach can precisely tailor the size, shape, geometrical features and mechanical stiffness of any type of microMESH and that each fabrication step can be tuned independently and separately.

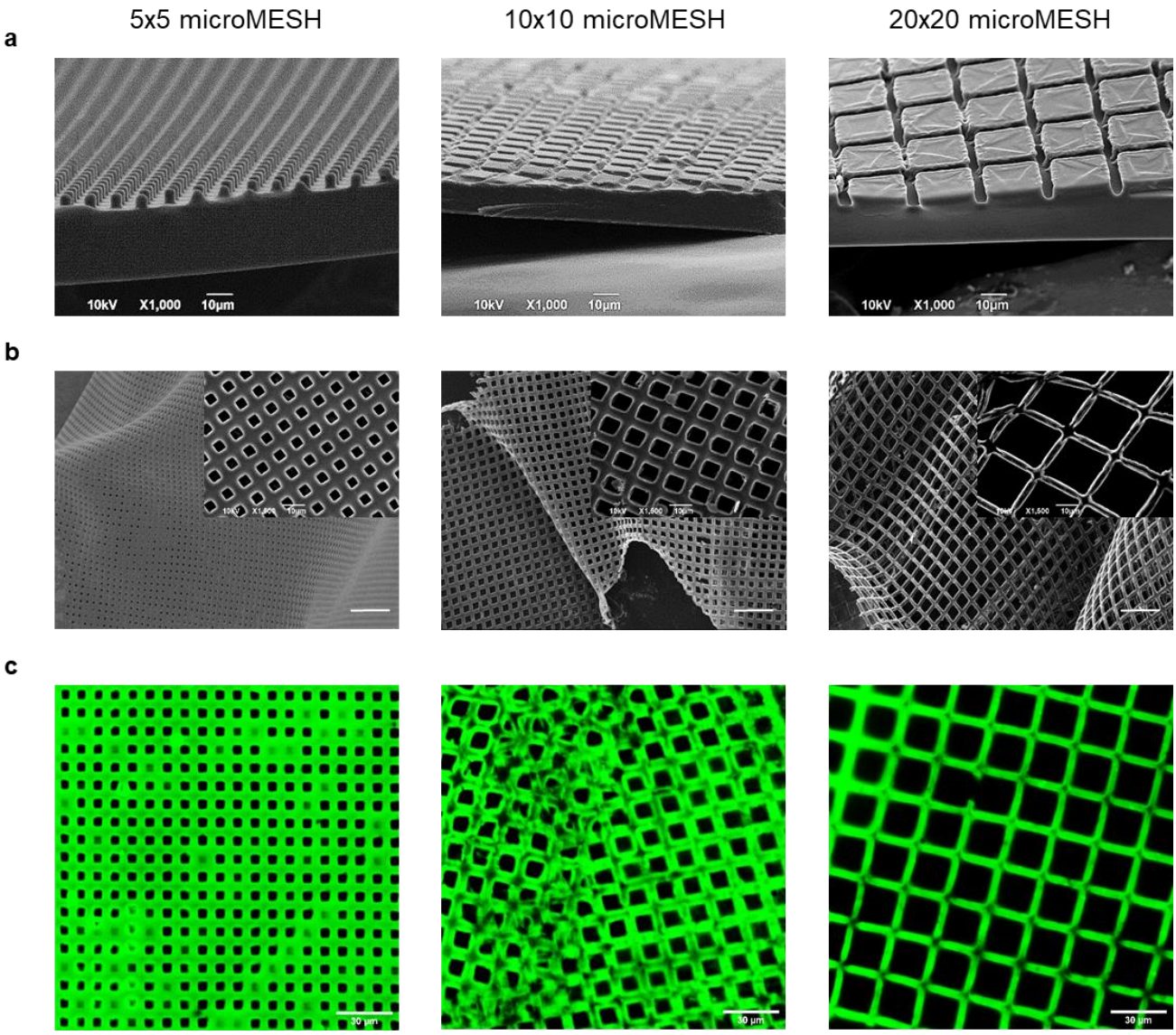

Figure 8. Geometrical characterization of the microMESH. a) The upper panel shows SEM images of the PVA template of the 5x5, 10x10 and 20x20 geometry. **b)** The middle panel shows from left to right 5x5, 10x10 and 20x20 microMESH, highlighting their peculiar flexibility (scale bar: 50µm). **c)** The bottom panel shows confocal microscopy images of Curcumin-loaded microMESH (green) of the same mentioned geometries.

hADSCs interaction with the microMESH

As shown in **Figure 9a**, cells grew uniformly distributed over the whole surface of the flat collagen scaffold adhering as a 2D monolayer; on the other hand, on top of the microMESH, the cells form

spheroidal-like aggregates. Indeed, the fluorescent microscopy and SEM images in **Figure 9b,** confirm that microMESH allows the cells to organize in assemblies. Additionally, as it possible to observe in the zoomed image (on the right middle panel) with its peculiar flexibility, the 20x20 microMESH enables the cells to stretch and crumple the net favoring a tight interaction with the substrate, which results incorporated within the 3D cell organization. The analysis of fluorescence microscopy images revealed that the number of spheroids formed on top of 5x5 microMESH was higher than the other geometries. On the contrary, on the 10x10 and 20x20 microMESH, the spheroids detected were lower at 24h. Anyway, in the latter geometries, this number remained almost constant over time. However, starting from a spheroids average size of 473,1 ± 253.3μm (5x5), 499,9 ± 199,3μm (10x10) and 423,7 ± 186.7μm (20x20) at 24h, they reached a perimeter of 470,7 ± 230,9μm (5x5), 467,4 ± 173,3μm (10x10) and 379,0 ± 158,5μm (20x20) at 48h and a final size of 476,0 ± 250,6μm (5x5), 441,3 ± 185,1μm (10x10) and 353,4 ± 144,3μm (20x20) in the last time point observed. Interestingly, for all the geometries, the aspect ratio seemed to tend towards the unit over time (**Figure 9c**).

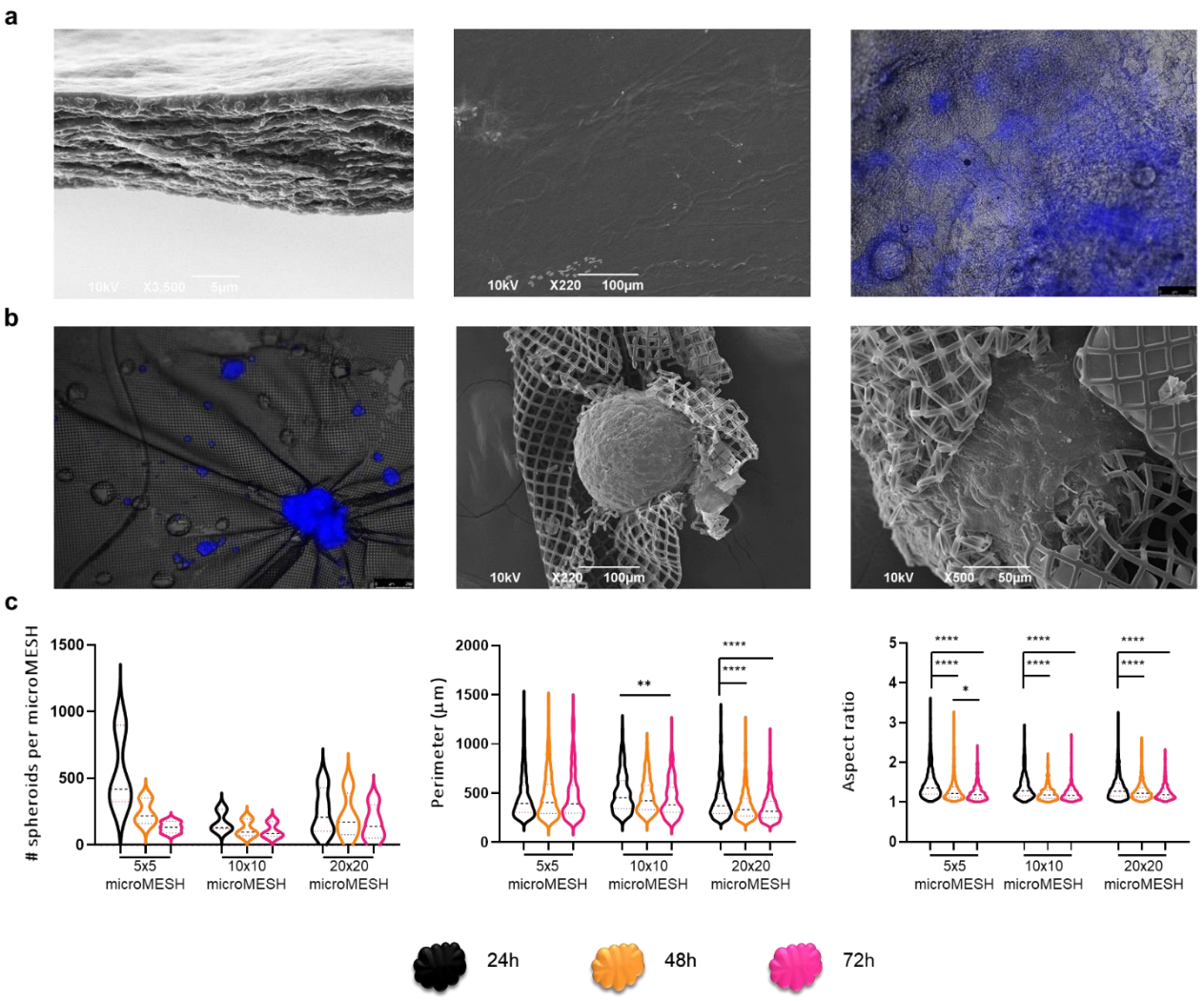

Figure 9. Analysis of spheroids growth over time. a) From left to right SEM images showing the transversal section (left) and the continuous surface (middle) of the collagen scaffold, whilst the fluorescence microscopy image (right) demonstrate cells adhered in 2D monolayer over the collagen sheet**. b)** The fluorescent microscopy image (left) displays the cells arranged into spheroids on top of 20x20 microMESH, whereas SEM images (middle and right) confirms the incorporation of the 20x20 microMESH within the structure of the spheroid. **c)** Spheroids characterization in terms of number of spheroids per microMESH, perimeter and aspect ratio at different time points, namely 24, 48 and 72h. Data are presented as mean ± SD. Each experiment was repeated multiple times independently (n ≥3). Differences are considered statistically significant when returning a p<0.05 (*), p<0.01 (**) and p<0,0001 (****).

Spheroid-derived hADSCs viability analysis

The hADSCs viability was evaluated in comparisons to cells grown on a plastic dish and on top of the collagen scaffold (the control conditions). Flow cytometry assay measured live, apoptotic and dead cells. Live cells showed no fluorescent signal, Annexin V-FITC stained apoptotic cells and PI stained dead cells. The results show that spheroids-derived hADSCs presented a similar percentage of live cells (e.g. around 80%) among the 5x5, 10x10 and 20x20 geometry. The result was comparable to the viability of hADSCs seeded on top of collagen scaffold. This was true at 24, 48 and 72h, despite the potential necrotic core formation within the structure of the spheroids caused by limited distribution of oxygen, nutrients and metabolites in the internal part of the cell assemble (**Figure 10**).

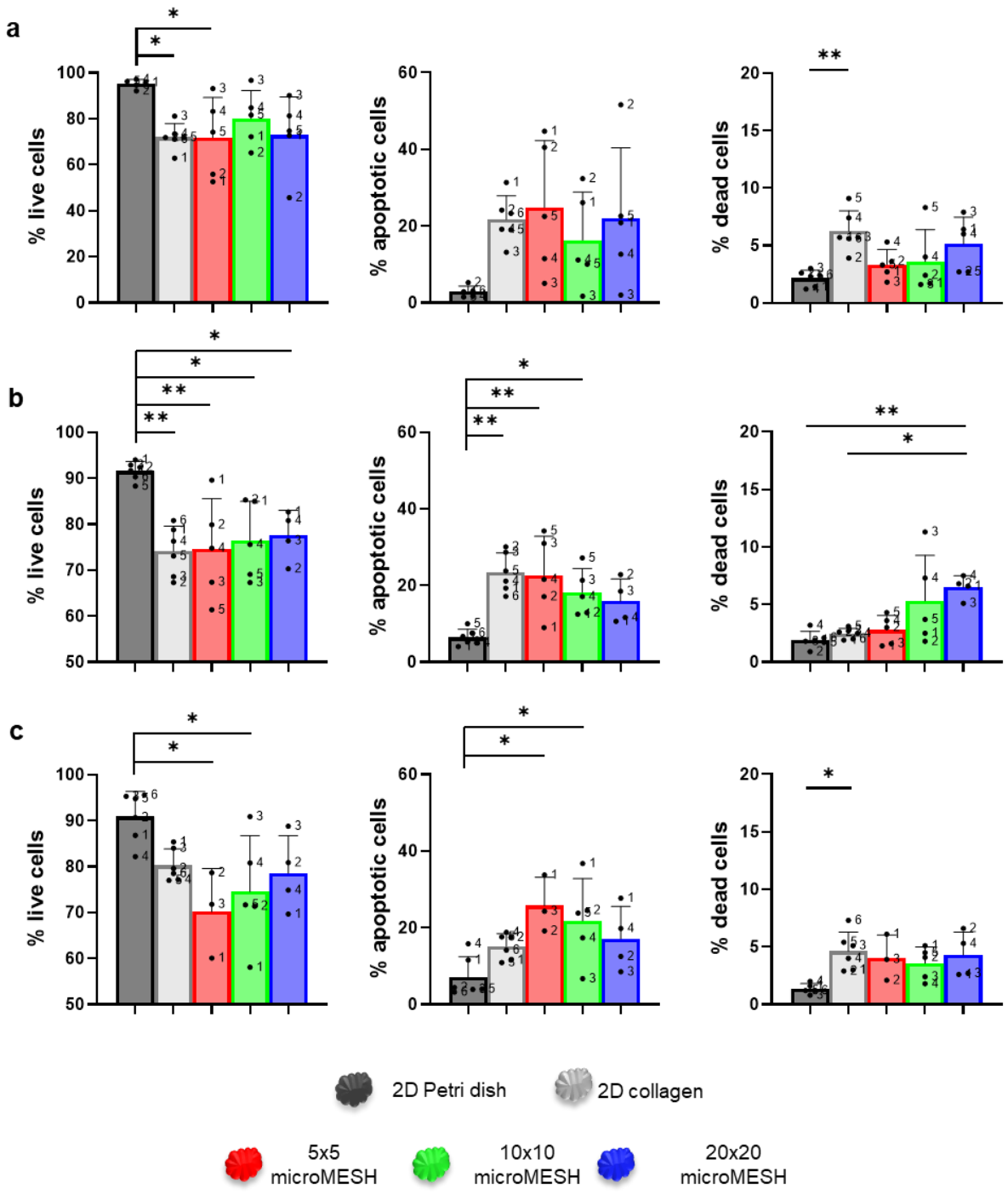

Figure 10. Cell viability. hADSCs viability in 2D and 3D cultures at **a)** 24h **b)** 48h and **c)** 72h. Data are presented as mean ± SD. Each experiment was repeated multiple times independently (n ≥3). Differences were considered statistically significant when returning a p value lower than 0.05 (*) and lower than 0.01 (**).

Actin reorganization during hADSCs interaction with microMESH

Cells were stained with Phalloidin-488 to observe and quantify actin conformations in all samples, including 2D Petri dish, 2D collagen and 5x5, 10x10 and 20x20 microMESH. Visual differences exist in the actin cytoskeleton organization among cell monolayers and spheroids-forming cells (**Figure 11a**). In the first conditions, actin fibers mainly present a linear shape with the 75% of the total amount of actin objects detected having an aspect ratio major than 5. On the contrary, once the cells were placed on top of the microMESH, the actin changed its shape resulting in nonlinear and less organized fibers. In particular, at the anchorage site to the PLGA mesh, despite the geometry, actin formed ring structures around the thin polymeric strands exploiting the openings in the microMESH geometries. Changes in actin structure reflect specific changes in cellular shape. Indeed, when they were seeded on top of microMESH, hADSCs assemble in spheroids. The histograms show the quantification of actin distribution within the cells in linear and nonlinear shape among the different substrates. The results demonstrated that in each microMESH geometries, the linear component never reached the 10% of the total actin within the cells, whereas this represents around the 80% in the both 2D Petri dish and 2D collagen conditions (**Figure 11b**).

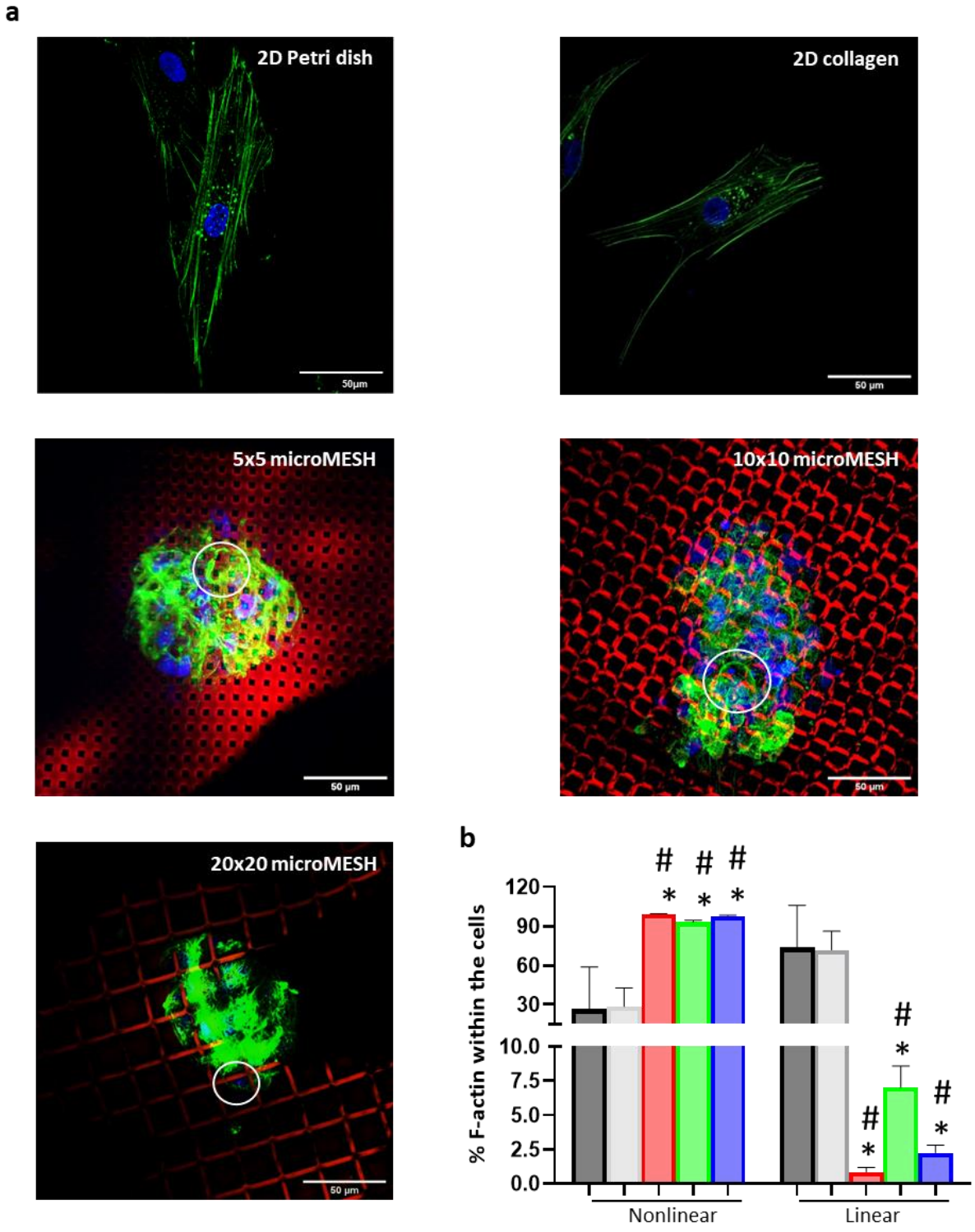
a
2D Petri dish
50µm
2D collagen
50 µm
5x5 microMESH
50 µm
10x10 microMESH
50 µm
20x20 microMESH
50 µm
b
% F-actin within the cells
120
90
60
30
10.0
7.5
5.0
2.5
0.0
Nonlinear
Linear
2D Petri dish
2D collagen
5x5 microMESH
10x10 microMESH
20x20 microMESH

Figure 11. hADSCs cytoskeleton organization. a) Confocal microscopy images show cells adhered in 2D monolayer in a Petri dish and on top of a collagen scaffold, and arranged into spheroids over the 5x5, 10x10 and 20x20 microMESH. **b**) Quantification of actin distribution within the cells. * represents a statistical significant difference compared to 2D Petri dish ($p<0.05$). # represents a statistical significant difference compared to collagen scaffold ($p<0.05$) ($n>3$).

Analysis of hADSCs secretome exposed to pro inflammatory stimulus

To determine the influence of the microMESH geometry on the paracrine activity of hADSCs, 48h after seeding the supernatants were collected and analyzed using a cytokine arrays. Particularly, in this study, we investigated if microMESH geometry could potentiate the release of some factors. Among the cytokines and chemokines detected by the kit a particular attention was given to those involved in angiogenesis, stem cell proliferation and cell survival, inflammation modulation, ECM remodeling, stem cell homing and promoting chemotaxis. All these processes are important for the treatment of MI.

Interestingly, 5x5 geometry proved its positive contribution in angiogenesis; indeed, significantly higher VEGF secretion level, was found in 5x5 configuration compared to the other conditions. Particularly, a statistically significant difference ($p<0.01$) was detected comparing 5x5 geometry and 2D Petri dish. Additionally, highest amounts of TIMP-2 and GCSF were detected in 5x5 geometry compared to the other conditions. Actually, 5x5 microMESH improved of 60% the secretion of TIMP-2 ($p<0.01$), involved in ECM remodeling and wound healing, compared to 2D collagen condition and raised by 20-fold the secretion of GCSF ($p<0.05$), involved in stimulating the bone marrow to deliver stem cells into the bloodstream, compared to 2D Petri dish. Notably, 5x5 configuration also elicited the production of TGF-β1, IL-10 and RANTES compared with control conditions demonstrating its participation in immuno-modulation and chemotaxis.

Further, 10x10 microrMESH is involved in promoting angiogenesis too. In fact, a significantly higher VEGF secretion level, was detected in 10x10 geometry when compared with 2D Petri condition ($p<0.05$) by one-way ANOVA with Tukey multiple comparison. This configuration also enhanced the release of FGF-family and EGF, implicated in stem cell proliferation and cell survival, respectively, when compared to 2D collagen condition, although without statistically significant differences. On the other hand, a significant increase of TIMP-2 secretion was found in the 10x10 geometry compared with 2D collagen condition ($p<0.05$). While no statistically significant differences were detected in the secretion of IL-10 and TGF-β1, we observed an increasing trend of those immune-modulatory factors with an anti-inflammatory effect, in 10x10 geometry when compared to 2D collagen condition.

Finally, 20x20 microMESH is manly implicated in ECM remodeling compared to the other processes; indeed it enhanced by 40% ($p<0.05$) the TIMP-2 production compared to 2D collagen condition. Moreover, slightly increased the secretion of IL-10 and RANTES compared to 2D collagen condition, demonstrating its participation in immune-system regulation and chemotaxis, although no statistically significant differences were detected among the conditions (**Figure 12**).

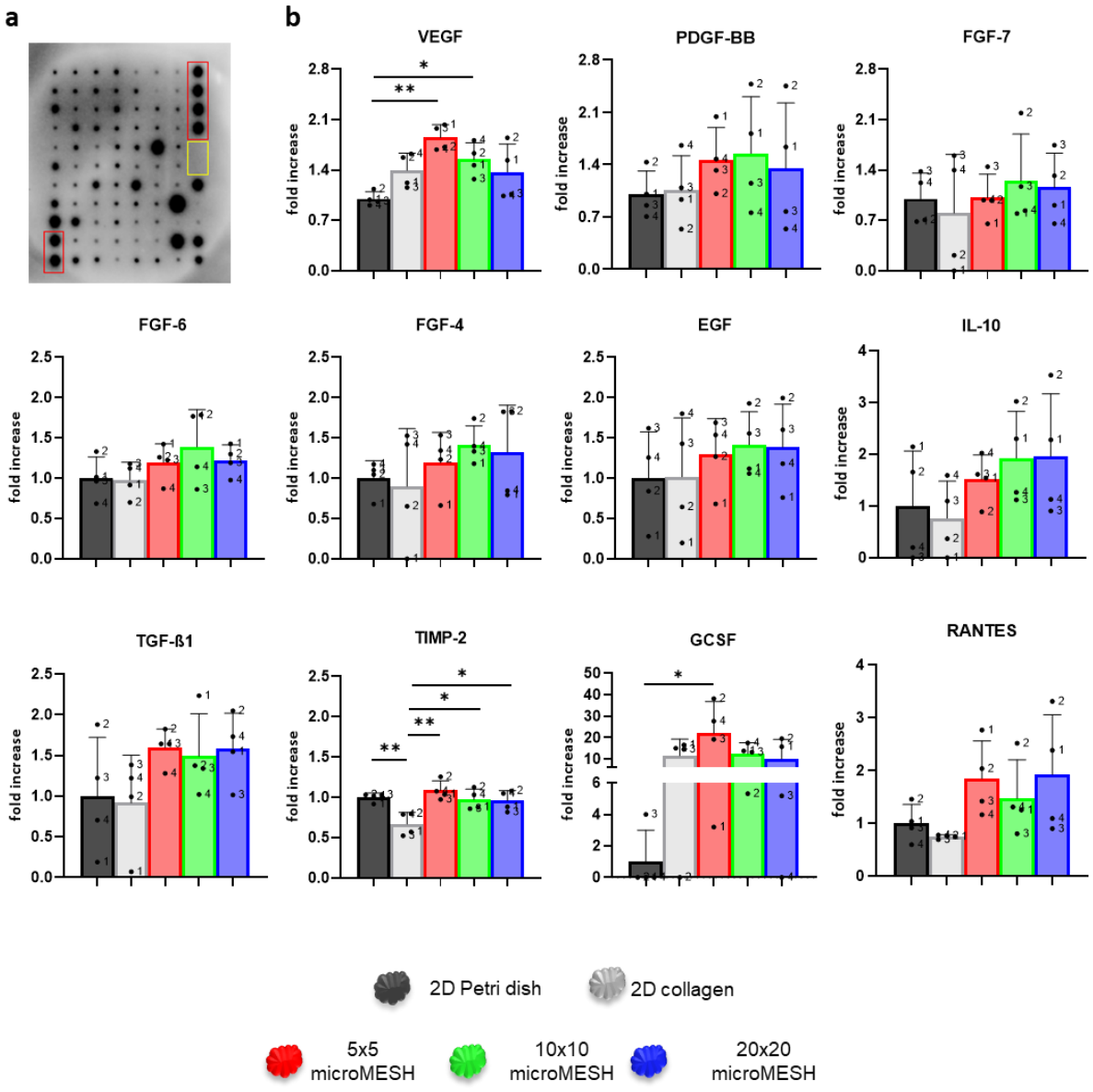

Figure 12. Analysis of hADSCs secretome exposed to TNF-α stimulation. a) Membrane array in which are underlined the negative (in yellow) and the positive (in red) control spots. **b)** Quantification of the cytokines' expression levels among the different scaffolds at 48h. Data are presented as mean ± SD. Each experiment was repeated multiple times independently (n ≥3). Differences are considered statistically significant when returning a $p<0.05$ (*) and $p< 0.01$ (**).

Phenotypic characterization of spheroid-forming hADSCs

The hADSC immunophenotype cultured on collagen scaffold and on top of the three types of microMESH were analyzed using flow cytometry. For this experiment, we evaluated the mean fluorescent increase compared to the mean fluorescence of the negative control as the parameter to compare the stemness markers expression levels on hADSCs surface. The analysis showed that hADSCs derived from spheroids disaggregation, over time tend to lose the expression of CD44, CD90 and CD105 markers as compared to the expression of those markers when the cells grown on top of collagen scaffold at the same time point. (**Figure 13**).

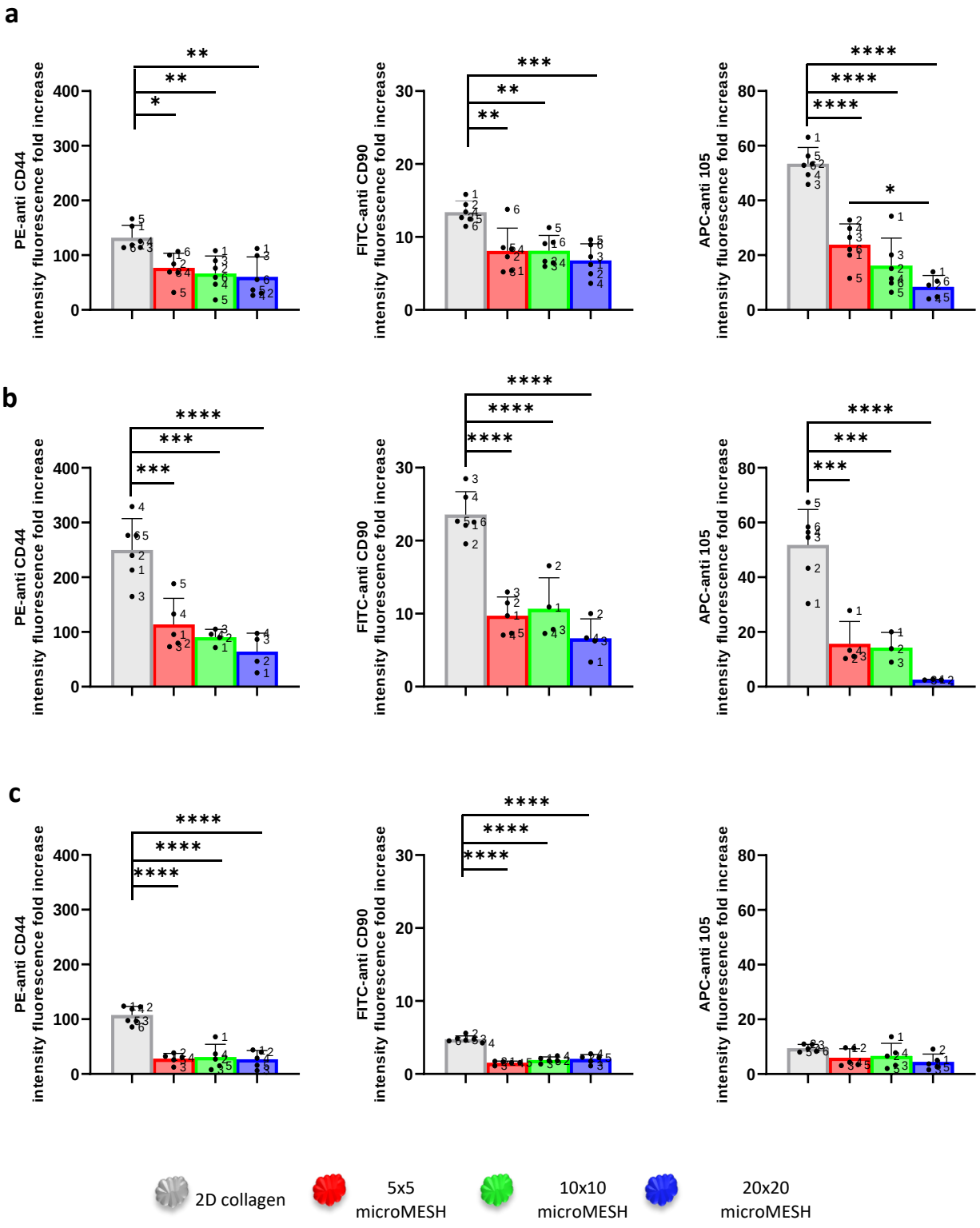

Figure 13. Flow cytometry analysis of stemness markers. In order, from left to right the fluorescence associated to CD44, CD90 and CD105 at **a)** 24h, **b)** 48h and **c)** 72h. Each bar represents the mean of almost four repetitions ±

SD. Differences are considered statistically significant when returning a p value<0.05 (*), p< 0.01(**), p< 0.001 (***) and p<0.0001 (****).

2.5. Discussion

The flexible device microMESH is designed to realize a suitable support for stem cell transplantation in the infarcted heart. The microMESH is fabricated employing silicon microchip technologies and polymer chemistry, returning a scaffold with precise geometry and physico-chemical features. The top-down fabrication strategy includes different steps whereby specific geometrical features are transferred from a silicon master template to a PVA layer passing through an intermediate polydimethylsiloxane (PDMS) template. On the final PVA layer, a polymeric PLGA paste is uniformly dispersed to accurately fill up the empty ridges between the micropillars. Both PLGA and PVA are biocompatible, biodegradable and FDA-approved materials, which means that in time they will be eliminated from the body, without inducing any significant toxicity.

Upon solvent evaporation, a solid PLGA mesh is returned comprising a regular network of polymeric strands with square openings of 5x5, 10x10 and 20x20 μm^2. These thin scaffolds are very flexible, as they could deforms and tightly conforms and adhere with the tissues in the implantation site, key feature for regenerative medicine application. Moreover, thanks to their peculiar general structures with multiple openings separated by narrow strands, the PLGA meshes can establish an intimate interaction with hADSCs. Indeed a very distinctive feature of this device is that each designed microMESH geometry allows hADSCs, seeded on top of it, to form spontaneously 3D spheroidal-like structures.

The relationship between the number of seeded cells and the number of spheroids formed over time on top of the microMESH could depend on different factors. Most likely, the more relevant

one is the number of cells available to form spheroids, which may be reduced by cell loss, because of the difference in the squared holes size in the three specific geometries of the microMESH. On the other hand, the strength of the interaction among hADSCs and the substrates could play an important role too. Indeed, the number of spheroids detected at 24h was higher in the 5x5 compared to the other geometries, probably because the smaller openings hampered the passage of the single cells through its spaces. Conversely, on top of the 10x10 and 20x20 microMESH, this number was lower at 24h compared to 5x5 geometry, because of a much higher possibility for the cells to pass through the bigger holes and deposit on the bottom of the Petri plate. Anyway, at 72h the number of spheroids anchored on top of 5x5 microMESH was lower than the ones observed over the 20x20 geometry, suggesting a more tightly interaction of the spheroids with the latter microMESH configuration. Hence, spheroids seems to adhered less stably to the 5x5 microMESH. Moreover, the perimeter did not change over time, suggesting that the aggregation process, which causes a shrinkage of the spheroids structure, balanced proliferation. Interestingly, spheroids tend to collapse their shape in a more spherical one, compared to an elongated organization at 24h. Over time the survival of spheroids-derived hADSCs was not compromised compared to 2D collagen scaffold.

Spheroids formation is induced by cytoskeleton rearrangement. The cytoskeleton, a complex web distributed throughout the cytoplasm, links the nucleus to the ECM and it is composed of different molecules, including actin. It changes in response to several stimuli, such as the geometry substrate, which may generate a reorganization of the actin structure inside the cells. This feature provides the cells the capability to adapt to an evolving microenvironment. In the common 2D monolayer culture the actin cytoskeleton is unidirectionally aligned [127]. Consistently, in our study, we found that hADSCs seeded on top of flat collagen layer adhered as a monolayer and actin cytoskeleton formed linear filaments. Conversely, once the hADSCs are placed on microMESH, the actin cytoskeleton reorganizes to confer a 3D cell shape with multidirectional

actin arrangement, forming nonlinear structures and ring structures at the anchorage site to the microMESH.

Morphological variation in MSCs acquired through cell-substrate and cell-cell interactions can exert beneficial paracrine effects [133]. However, the influence of materials on cells behavior is intricate, and much is unknown on how cells should be handle to achieve the optimal cell function and thereby therapeutic outcome *in vivo* [134]. Anyway, by profiling the secretome of hADSCs cultured in different substrates, our study indicates that microMESH geometry provided a unique microenvironment that could enhance the hADSCs paracrine secretion. Specifically, it has emerged that, when cultured on microMESH, there was a trend for higher production of several factors with specific implications in angiogenesis (e.g. VEGF, PDGF-BB), stem cell proliferation and expansion (e.g. FGFs-family), cell survival (e.g. EGF), inflammation modulation (e.g. IL-10 and TGF-β1), ECM remodeling (e.g. TIMP-2), stem cell mobilization, chemotaxis and homing (e.g. GCSF and RANTES), as compared to 2D Petri dish and 2D collagen conditions.

In the end, we started to study some markers on spheroids-derived hADSCs cells surface, by fluorescence-activated cell sorting (FACS). The initial candidates were the peculiar hADSCs stemness markers, namely CD44, CD90 and CD105, and our preliminary results highlights that microMESH compromised the expression of such markers compared to the collagen scaffold over time. This is a very interesting outcome, as in general 3D cell culture systems preserve the multilineage potential of mesenchymal stem cells. On the other hand, actin cytoskeleton participates in cell differentiation process [135],[136], which could explain the reduction of CD44, CD90 and CD105 expression levels we obtained on microMESH compared to the outcomes we found on 2D collagen condition; meaning the peculiar arrangement on microMESH can favor hADSCs differentiation. However, some limitations of this study should be mentioned. To perform the stemness study on microMESH, per each replicate were used 7 millions of cells in order to compensate the loss of the cells passing through its holes and at the same time having a proper

number to perform the consequent flow cytometry analysis. Thus, to realize all the replicates, and collect this huge amount of cells, they were expanded in flask until passage 12. On the contrary, to perform stemness study on collagen the cells were expanded for 2 weeks in flask until passage 7, because the number of cells required for the analysis was extremely reduced. We believed that this mismatch in cell passage could be one of the reasons that determined the results. This is why we are continuing to investigate more over this study. Eventually, we will consider quantifying other markers that can suggest a hADSCs specific cellular commitment.

Chapter 3

3.1. Conclusions and future outlook

The project rationale was to create a suitable substrate, which might favors cell survival and engraftment to the heart for MI treatment. By taking advantage of the accurate size, shape, surface proprieties and mechanical stiffness control offered by the top-down fabrication technique, we were able to fabricate three different microMESH types named 5x5, 10x10 and 20x20. Indeed, the microMESH structure comprises a regular network of evenly spaced 5, 10 and 20 μm holes respectively, resulting in a regular micro-sized network just like a fishing net. Furthermore, each microMESH revealed to be an effective support for the cells being biocompatible and biodegradable. Unlike collagen, which was not stretched or deformed by hADSCs, microMESH established an intimate interaction with the cells. In fact, it resulted incorporated within the 3D structures formed by the cells cultured on top of it. Whereas, such cells, adhered forming a common monolayer over the collagen scaffold. Anyway, in both scaffolds cells over time presented a good viability. Notably, from several previous studies, this peculiar perspective of the microMESH seems to match perfectly with the preferable 3D culture systems for a better reproduction of the native human heart.

Investigations over the actin cytoskeleton organization on microMESH demonstrated that geometry influences its arrangement, which was predominantly organized in nonlinear actin fibers. Then we focused on the correlation between geometry and biological behavior of hADSCs. Therefore, we analyzed the cytokine secretion profiles for all three different microMESH in order to understand if geometry could influence the paracrine activity of hADSCs. Our results assessed the beneficial effects achieved by 5x5, 10x10 and 20x20 geometry on increasing the secretion of

several factors involved in key biological processes for MI resolution, such as angiogenesis, cell proliferation and survival, ECM remodeling, stem cell homing, and anti-inflammatory effect.

Interestingly, geometry microMESH seems to have an influence also on the hADSCs stamness at least for the evaluated markers, namely CD44, CD90 and CD105. However, more work need to be done to better interpret these outcomes and more markers need to be characterized. In the future, we will focus more on stemness study in order to understand if hADSCs have reached a certain cellular commitment. We would also examine co-culturing conditions to understand if microMESH geometry can promote cardiomyocytes survival and proliferation through the increased production of paracrine factors.

References

[1] V. F. M. Segers and R. T. Lee, “Stem-cell therapy for cardiac disease,” *Nature*, vol. 451, no. 7181, pp. 937–942, 2008, doi: 10.1038/nature06800.

[2] R. Gong, Z. Jiang, N. Zagidullin, T. Liu, and B. Cai, “Regulation of cardiomyocyte fate plasticity: a key strategy for cardiac regeneration,” *Signal Transduct. Target. Ther.*, vol. 6, no. 1, 2021, doi: 10.1038/s41392-020-00413-2.

[3] Y. Guo, Y. Yu, S. Hu, Y. Chen, and Z. Shen, “The therapeutic potential of mesenchymal stem cells for cardiovascular diseases,” *Cell Death Dis.*, vol. 11, no. 5, 2020, doi: 10.1038/s41419-020-2542-9.

[4] T. J. Streef and A. M. Smits, “Epicardial Contribution to the Developing and Injured Heart: Exploring the Cellular Composition of the Epicardium,” *Front. Cardiovasc. Med.*, vol. 8, no. September, pp. 1–16, 2021, doi: 10.3389/fcvm.2021.750243.

[5] A. Diaz-Pinto *et al.*, “Predicting myocardial infarction through retinal scans and minimal personal information,” *Nat. Mach. Intell.*, vol. 4, no. 1, pp. 55–61, 2022, doi: 10.1038/s42256-021-00427-7.

[6] S. Vukicevic *et al.*, “Bone morphogenetic protein 1.3 inhibition decreases scar formation and supports cardiomyocyte survival after myocardial infarction,” *Nat. Commun.*, vol. 13, no. 1, pp. 1–11, 2022, doi: 10.1038/s41467-021-27622-9.

[7] M. Litviňuková *et al.*, “Cells of the adult human heart,” *Nature*, vol. 588, no. 7838, pp. 466–472, 2020, doi: 10.1038/s41586-020-2797-4.

[8] M. Giacca, “Cardiac Regeneration After Myocardial Infarction: an Approachable Goal,” *Curr. Cardiol. Rep.*, vol. 22, no. 10, 2020, doi: 10.1007/s11886-020-01361-7.

[9] T. J. Cahill, R. P. Choudhury, and P. R. Riley, “Heart regeneration and repair after myocardial infarction: Translational opportunities for novel therapeutics,” *Nat. Rev. Drug Discov.*, vol. 16, no. 10, pp. 699–717, 2017, doi: 10.1038/nrd.2017.106.

[10] M. A. Laflamme and C. E. Murry, “Heart Regenartion,” *Nature*, vol. 23, no. 1, pp. 1–7, 2011, doi: 10.1038/nature10147.Heart.

[11] J. Cho *et al.*, “Regeneration of infarcted mouse hearts by cardiovascular tissue formed via the direct reprogramming of mouse fibroblasts,” *Nat. Biomed. Eng.*, vol. 5, no. 8, pp. 880–896, 2021, doi: 10.1038/s41551-021-00783-0.

[12] P. Mirmiran, F. Hosseini-Esfahani, Z. Esfandiar, S. Hosseinpour-Niazi, and F. Azizi, “Associations between dietary antioxidant intakes and cardiovascular disease,” *Sci. Rep.*, vol. 12, no. 1, pp. 1–11, 2022, doi: 10.1038/s41598-022-05632-x.

[13] R. B. D’Agostino *et al.*, “General cardiovascular risk profile for use in primary care: The Framingham heart study,” *Circulation*, vol. 117, no. 6, pp. 743–753, 2008, doi: 10.1161/CIRCULATIONAHA.107.699579.

[14] K. Thygesen *et al.*, *Fourth Universal Definition of Myocardial Infarction (2018)*, vol. 138, no. 20. 2018.

[15] S. Mattapally *et al.*, “Spheroids of cardiomyocytes derived from human-induced pluripotent stem cells improve recovery from myocardial injury in mice,” *Am. J. Physiol. - Hear. Circ. Physiol.*, vol. 315, no. 2, pp. H327–H339, 2018, doi: 10.1152/ajpheart.00688.2017.

[16] B. Ibanez *et al.*, “2017 ESC Guidelines for the management of acute myocardial infarction in patients presenting with ST-segment elevation,” *Eur. Heart J.*, vol. 39, no. 2, pp. 119–177, 2018, doi: 10.1093/eurheartj/ehx393.

[17] C. Prevention *et al.*, “2016 European Guidelines on cardiovascular disease prevention in clinical practice The Sixth Joint Task Force of the European Society of Cardiology,” pp. 2315–2381, 2016, doi: 10.1093/eurheartj/ehw106.

[18] R. Mehta *et al.*, “Dose Comparisons of Clopidogrel and Aspirin in Acute Coronary Syndromes,” 2010.

[19] C. T. Trialists, “Efficacy and safety of cholesterol-lowering treatment : prospective meta-analysis of data from 90 056 participants in 14 randomised trials of statins,” pp. 1267–1278, 1994, doi: 10.1016/S0140-6736(05)67394-1.

[20] M. D. Epelman S, Liu P, “Role of Innate and Adaptive Immunity in Cardiac Injury and Repair,” *Narure Rev. Immunol.*, vol. 15, no. 2, pp. 117–129, 2015, doi: 10.1038/nri3800.Role.

[21] L. Adamo, C. Rocha-Resende, S. D. Prabhu, and D. L. Mann, “Reappraising the role of inflammation in heart failure,” *Nat. Rev. Cardiol.*, vol. 17, no. 5, pp. 269–285, 2020, doi: 10.1038/s41569-019-0315-x.

[22] S. D. Prabhu and N. G. Frangogiannis, “The biological basis for cardiac repair after myocardial infarction,” *Circ. Res.*, vol. 119, no. 1, pp. 91–112, 2016, doi: 10.1161/CIRCRESAHA.116.303577.

[23] H. Abe *et al.*, “NF-κB activation in cardiac fibroblasts results in the recruitment of inflammatory Ly6Chi monocytes in pressure-overloaded hearts,” *Sci. Signal.*, vol. 14, no. 704, pp. 1–11, 2021, doi: 10.1126/SCISIGNAL.ABE4932.

[24] S. W. M. Van Den Borne, J. Diez, W. M. Blankesteijn, J. Verjans, L. Hofstra, and J. Narula, “Myocardial remodeling after infarction: The role of myofibroblasts,” *Nat. Rev. Cardiol.*, vol. 7, no. 1, pp. 30–37, 2010, doi: 10.1038/nrcardio.2009.199.

[25] X. Wu, M. R. Reboll, M. Korf-Klingebiel, and K. C. Wollert, “Angiogenesis after acute myocardial infarction,” *Cardiovasc. Res.*, vol. 117, no. 5, pp. 1257–1273, 2021, doi: 10.1093/cvr/cvaa287.

[26] D. Fraccarollo, P. Galuppo, and J. Bauersachs, “Novel therapeutic approaches to post-infarction remodelling,” *Cardiovasc. Res.*, vol. 94, no. 2, pp. 293–303, 2012, doi: 10.1093/cvr/cvs109.

[27] Q. Zhang *et al.*, “Signaling pathways and targeted therapy for myocardial infarction,” *Signal Transduct. Target. Ther.*, vol. 7, no. 1, 2022, doi: 10.1038/s41392-022-00925-z.

[28] B. Nadal-Ginard, J. Kajstura, A. Leri, and P. Anversa, “Myocyte death, growth, and regeneration in cardiac hypertrophy and failure,” *Circ. Res.*, vol. 92, no. 2, pp. 139–150, 2003, doi: 10.1161/01.RES.0000053618.86362.DF.

[29] P. Anversa, J. Kajstura, A. Leri, and R. Bolli, “Life and death of cardiac stem cells: A paradigm shift in cardiac biology,” *Circulation*, vol. 113, no. 11, pp. 1451–1463, 2006, doi: 10.1161/CIRCULATIONAHA.105.595181.

[30] D. Torella, G. M. Ellison, S. Méndez-Ferrer, B. Ibanez, and B. Nadal-Ginard, “Resident human cardiac stem cells: Role in cardiac cellular homeostasis and potential for myocardial regeneration,” *Nat. Clin. Pract. Cardiovasc. Med.*, vol. 3, no. SUPPL. 1, pp. 8–13, 2006, doi: 10.1038/ncpcardio0409.

[31] A. P. Beltrami *et al.*, “Adult Cardiac Stem Cells Are Multipotent and Support Myocardial Regeneration we have documented the existence of cycling ventricu- lar myocytes in the normal and pathologic adult mam,” *Cell*, vol. 114, pp. 763–776, 2003.

[32] L. Macri-Pellizzeri, E. M. De-Juan-Pardo, F. Prosper, and B. Pelacho, “Role of substrate biomechanics in controlling (stem) cell fate: Implications in regenerative medicine,” *J.*

Tissue Eng. Regen. Med., vol. 12, no. 4, pp. 1012–1019, 2018, doi: 10.1002/term.2586.

[33] R. Mazhari and J. M. Hare, “Mechanisms of action of mesenchymal stem cells in cardiac repair: Potential influences on the cardiac stem cell niche,” *Nat. Clin. Pract. Cardiovasc. Med.*, vol. 4, no. SUPPL. 1, pp. 21–26, 2007, doi: 10.1038/ncpcardio0770.

[34] Z. Lin and W. T. Pu, “Strategies for cardiac regeneration and repair,” *Sci. Transl. Med.*, vol. 6, no. 239, pp. 1–12, 2014, doi: 10.1126/scitranslmed.3006681.

[35] N. M. Caplice, B. J. Gersh, and J. R. Alegria, “Cell therapy for cardiovascular disease: What cells, what diseases and for whom?,” *Nat. Clin. Pract. Cardiovasc. Med.*, vol. 2, no. 1, pp. 37–43, 2005, doi: 10.1038/ncpcardio0073.

[36] B. E. Strauer *et al.*, “Repair of infarcted myocardium by autologous intracoronary mononuclear bone marrow cell transplantation in humans,” *Circulation*, vol. 106, no. 15, pp. 1913–1918, 2002, doi: 10.1161/01.CIR.0000034046.87607.1C.

[37] B. Assmus *et al.*, “Transplantation of progenitor cells and regeneration enhancement in acute myocardial infarction (TOPCARE-AMI),” *Circulation*, vol. 106, no. 24, pp. 3009–3017, 2002, doi: 10.1161/01.CIR.0000043246.74879.CD.

[38] M. Yousef, C. M. Schannwell, M. Köstering, T. Zeus, M. Brehm, and B. E. Strauer, “The BALANCE Study,” *J. Am. Coll. Cardiol.*, vol. 53, no. 24, pp. 2262–2269, 2009, doi: 10.1016/j.jacc.2009.02.051.

[39] D. Orlic, J. Kajstura, S. Chimenti, D. M. Bodine, A. Leri, and P. Anversa, “Bone marrow stem cells regenerate infarcted myocardium,” *Pediatr. Transplant.*, vol. 7, no. SUPPL. 3, pp. 86–88, 2003, doi: 10.1034/j.1399-3046.7.s3.13.x.

[40] S. A. Fisher, H. Zhang, C. Doree, A. Mathur, and E. Martin-Rendon, “Stem cell treatment for acute myocardial infarction,” *Cochrane Database Syst. Rev.*, vol. 2015, no. 9, 2015,

doi: 10.1002/14651858.CD006536.pub4.

[41] A. W. Heldman *et al.*, “Transendocardial mesenchymal stem cells and mononuclear bone marrow cells for ischemic cardiomyopathy: The TAC-HFT randomized trial,” *JAMA - J. Am. Med. Assoc.*, vol. 311, no. 1, pp. 62–73, 2014, doi: 10.1001/jama.2013.282909.

[42] A. Attar, F. Bahmanzadegan Jahromi, S. Kavousi, A. Monabati, and A. Kazemi, “Mesenchymal stem cell transplantation after acute myocardial infarction: a meta-analysis of clinical trials,” *Stem Cell Res. Ther.*, vol. 12, no. 1, pp. 1–11, 2021, doi: 10.1186/s13287-021-02667-1.

[43] A. Attar *et al.*, “Single vs . double intracoronary injection of mesenchymal stromal cell after acute myocardial infarction : the study protocol from a randomized clinical trial : BOOSTER-,” pp. 4–11, 2022.

[44] J. M. Hare, J. E. Fishman, and Alan W. Heldman, “Comparison of Allogeneic vs Autologous Bone Marrow–Derived Mesenchymal Stem Cells Delivered by Transendocardial Injection in Patients With Ischemic Cardiomyopathy,” *J Autism Dev Disord*, vol. 47, no. 3, pp. 549–562, 2017, doi: 10.1001/jama.2012.25321.Comparison.

[45] Y. Miyahara *et al.*, “Monolayered mesenchymal stem cells repair scarred myocardium after myocardial infarction,” *Nat. Med.*, vol. 12, no. 4, pp. 459–465, 2006, doi: 10.1038/nm1391.

[46] T. Squillaro, G. Peluso, and U. Galderisi, “Clinical trials with mesenchymal stem cells: An update,” *Cell Transplant.*, vol. 25, no. 5, pp. 829–848, 2016, doi: 10.3727/096368915X689622.

[47] A. J. Friedenstein, R. K. Chailakhyan, N. V. Latsinik, A. F. Panasyuk, and I. V. Keiliss-Borok, “Stromal Cells Responsible for Transferring the Microenvironment of the

Hemopoietic Tissues," *Transplantation*, vol. 17, no. 4. pp. 331–340, 1974, doi: 10.1097/00007890-197404000-00001.

[48] Y. Han *et al.*, "The secretion profile of mesenchymal stem cells and potential applications in treating human diseases," *Signal Transduct. Target. Ther.*, vol. 7, no. 1, 2022, doi: 10.1038/s41392-022-00932-0.

[49] O. Levy *et al.*, "Shattering barriers toward clinically meaningful MSC therapies," *Sci. Adv.*, vol. 6, no. 30, pp. 1–19, 2020, doi: 10.1126/sciadv.aba6884.

[50] T. T. Tran and C. R. Kahn, "Transplantation of adipose tissue and stem cells: Role in metabolism and disease," *Nat. Rev. Endocrinol.*, vol. 6, no. 4, pp. 195–213, 2010, doi: 10.1038/nrendo.2010.20.

[51] M. Araña *et al.*, "Epicardial delivery of collagen patches with adipose-derived stem cells in rat and minipig models of chronic myocardial infarction," *Biomaterials*, vol. 35, no. 1, pp. 143–151, 2014, doi: 10.1016/j.biomaterials.2013.09.083.

[52] I. Perez-Estenaga, F. Prosper, and B. Pelacho, "Allogeneic mesenchymal stem cells and biomaterials: The perfect match for cardiac repair?," *Int. J. Mol. Sci.*, vol. 19, no. 10, 2018, doi: 10.3390/ijms19103236.

[53] M. Dominici *et al.*, "Minimal criteria for defining multipotent mesenchymal stromal cells. The International Society for Cellular Therapy position statement," *Cytotherapy*, vol. 8, no. 4, pp. 315–317, 2006, doi: 10.1080/14653240600855905.

[54] S. Viswanathan *et al.*, "Mesenchymal stem versus stromal cells: International Society for Cell & Gene Therapy (ISCT®) Mesenchymal Stromal Cell committee position statement on nomenclature," *Cytotherapy*, vol. 21, no. 10, pp. 1019–1024, 2019, doi: 10.1016/j.jcyt.2019.08.002.

[55] M. Gnecchi, Z. Zhang, A. Ni, and V. J. Dzau, “Paracrine mechanisms in adult stem cell signaling and therapy,” *Circ. Res.*, vol. 103, no. 11, pp. 1204–1219, 2008, doi: 10.1161/CIRCRESAHA.108.176826.

[56] H. C. Quevedo *et al.*, “Allogeneic mesenchymal stem cells restore cardiac function in chronic ischemic cardiomyopathy via trilineage differentiating capacity,” *Proc. Natl. Acad. Sci. U. S. A.*, vol. 106, no. 33, pp. 14022–14027, 2009, doi: 10.1073/pnas.0903201106.

[57] J. M. Nygren *et al.*, “Bone marrow-derived hematopoietic cells generate cardiomyocytes at a low frequency through cell fusion, but not transdifferentiation,” *Nat. Med.*, vol. 10, no. 5, pp. 494–501, 2004, doi: 10.1038/nm1040.

[58] K. E. Hatzistergos *et al.*, “Bone marrow mesenchymal stem cells stimulate cardiac stem cell proliferation and differentiation,” *Circ. Res.*, vol. 107, no. 7, pp. 913–922, 2010, doi: 10.1161/CIRCRESAHA.110.222703.

[59] I. Y. Shadrin, W. Yoon, L. Li, N. Shepherd, and N. Bursac, “Rapid fusion between mesenchymal stem cells and cardiomyocytes yields electrically active, non-contractile hybrid cells,” *Sci. Rep.*, vol. 5, no. March, pp. 20–22, 2015, doi: 10.1038/srep12043.

[60] J. Zeng, Y. Wang, Y. Wei, A. Xie, Y. Lou, and M. Zhang, “Co-culture with cardiomyocytes induces mesenchymal stem cells to differentiate into cardiomyocyte-like cells and express heart development-associated genes,” *Cell Res.*, vol. 18, no. S1, pp. S62–S62, 2008, doi: 10.1038/cr.2008.152.

[61] S. Rangappa, C. Fen, L. Eh, A. Bongso, and S. Ek, “Transformation of adult mesenchymal stem cells isolated from the fatty tissue into cardiomyocytes . PubMed Commons,” *Elsevier*, vol. 4975, no. 02, pp. 1–2, 2014, [Online]. Available: https://www.sciencedirect.com/science/article/pii/S000349750204568X.

[62] K. G. Gaustad, A. C. Boquest, B. E. Anderson, A. M. Gerdes, and P. Collas, "Differentiation of human adipose tissue stem cells using extracts of rat cardiomyocytes," *Biochem. Biophys. Res. Commun.*, vol. 314, no. 2, pp. 420–427, 2004, doi: 10.1016/j.bbrc.2003.12.109.

[63] V. Planat-Bénard *et al.*, "Spontaneous Cardiomyocyte Differentiation from Adipose Tissue Stroma Cells," *Circ. Res.*, vol. 94, no. 2, pp. 223–229, 2004, doi: 10.1161/01.RES.0000109792.43271.47.

[64] J. K. Fraser *et al.*, "Plasticity of human adipose stem cells toward endothelial cells and cardiomyocytes," *Nat. Clin. Pract. Cardiovasc. Med.*, vol. 3, no. SUPPL. 1, pp. 33–37, 2006, doi: 10.1038/ncpcardio0444.

[65] J. R. Lee *et al.*, "Nanovesicles derived from iron oxide nanoparticles-incorporated mesenchymal stem cells for cardiac repair," *Sci. Adv.*, vol. 6, no. 18, 2020, doi: 10.1126/sciadv.aaz0952.

[66] Y. R. Kim *et al.*, "Potential benefits of mesenchymal stem cells and electroacupuncture on the trophic factors associated with neurogenesis in mice with ischemic stroke," *Sci. Rep.*, vol. 8, no. 1, pp. 1–13, 2018, doi: 10.1038/s41598-018-20481-3.

[67] S. Gordon and A. Mantovani, "Diversity and plasticity of mononuclear phagocytes," *Eur. J. Immunol.*, vol. 41, no. 9, pp. 2470–2472, 2011, doi: 10.1002/eji.201141988.

[68] M. Najar, M. Krayem, N. Meuleman, D. Bron, and L. Lagneaux, "Mesenchymal stromal cells and toll-like receptor priming: A critical review," *Immune Netw.*, vol. 17, no. 2, pp. 89–102, 2017, doi: 10.4110/in.2017.17.2.89.

[69] Q. Zhao, H. Ren, and Z. Han, "Mesenchymal stem cells: Immunomodulatory capability and clinical potential in immune diseases," *J. Cell. Immunother.*, vol. 2, no. 1, pp. 3–20,

2016, doi: 10.1016/j.jocit.2014.12.001.

[70] A. Mantovani, S. K. Biswas, M. R. Galdiero, A. Sica, and M. Locati, “Macrophage plasticity and polarization in tissue repair and remodelling,” *J. Pathol.*, vol. 229, no. 2, pp. 176–185, 2013, doi: 10.1002/path.4133.

[71] M. E. Bernardo and W. E. Fibbe, “Mesenchymal stromal cells: Sensors and switchers of inflammation,” *Cell Stem Cell*, vol. 13, no. 4, pp. 392–402, 2013, doi: 10.1016/j.stem.2013.09.006.

[72] P. R. Crisostomo, Y. Wang, T. A. Markel, M. Wang, T. Lahm, and D. R. Meldrum, “Human mesenchymal stem cells stimulated by TNF-α, LPS, or hypoxia produce growth factors by an NFκB- but not JNK-dependent mechanism,” *Am. J. Physiol. - Cell Physiol.*, vol. 294, no. 3, pp. 675–682, 2008, doi: 10.1152/ajpcell.00437.2007.

[73] G. Ren *et al.*, “Mesenchymal Stem Cell-Mediated Immunosuppression Occurs via Concerted Action of Chemokines and Nitric Oxide,” *Cell Stem Cell*, vol. 2, no. 2, pp. 141–150, 2008, doi: 10.1016/j.stem.2007.11.014.

[74] M. Wang, Q. Yuan, and L. Xie, “Mesenchymal stem cell-based immunomodulation: Properties and clinical application,” *Stem Cells Int.*, vol. 2018, 2018, doi: 10.1155/2018/3057624.

[75] L. Zhu *et al.*, “TSC1 controls macrophage polarization to prevent inflammatory disease,” *Nat. Commun.*, vol. 5, 2014, doi: 10.1038/ncomms5696.

[76] E. Eggenhofer and M. J. Hoogduijn, “Mesenchymal stem cell-educated macrophages,” *Transplant. Res.*, vol. 1, no. 1, p. 1, 2012, doi: 10.1186/2047-1440-1-12.

[77] S. A. O’Rourke, A. Dunne, and M. G. Monaghan, “The Role of Macrophages in the Infarcted Myocardium: Orchestrators of ECM Remodeling,” *Front. Cardiovasc. Med.*, vol.

6, no. July, pp. 1–12, 2019, doi: 10.3389/fcvm.2019.00101.

[78] N. Su, Y. Hao, F. Wang, W. Hou, H. Chen, and Y. Luo, “Mesenchymal stromal exosome–functionalized scaffolds induce innate and adaptive immunomodulatory responses toward tissue repair,” *Sci. Adv.*, vol. 7, no. 20, pp. 1–13, 2021, doi: 10.1126/sciadv.abf7207.

[79] S. P. Burr, F. Dazzi, and O. A. Garden, “Mesenchymal stromal cells and regulatory T cells: The Yin and Yang of peripheral tolerance,” *Immunol. Cell Biol.*, vol. 91, no. 1, pp. 12–18, 2013, doi: 10.1038/icb.2012.60.

[80] K. A. Cho, J. K. Lee, Y. H. Kim, M. Park, S. Y. Woo, and K. H. Ryu, “Mesenchymal stem cells ameliorate B-cell-mediated immune responses and increase IL-10-expressing regulatory B cells in an EBI3-dependent manner,” *Cell. Mol. Immunol.*, vol. 14, no. 11, pp. 895–908, 2017, doi: 10.1038/cmi.2016.59.

[81] B. W. Park *et al.*, “In vivo priming of human mesenchymal stem cells with hepatocyte growth factor–engineered mesenchymal stem cells promotes therapeutic potential for cardiac repair,” *Sci. Adv.*, vol. 6, no. 13, 2020, doi: 10.1126/sciadv.aay6994.

[82] G. Liu *et al.*, “A VEGF delivery system targeting MI improves angiogenesis and cardiac function based on the tropism of MSCs and layer-by-layer self-assembly,” *Biomaterials*, vol. 127, pp. 117–131, 2017, doi: 10.1016/j.biomaterials.2017.03.001.

[83] E. E. J. M. Creemers, J. P. M. Cleutjens, J. F. M. Smits, and M. J. A. P. Daemen, “Matrix metalloproteinase inhibition after myocardial infarction: A new approach to prevent heart failure?,” *Circ. Res.*, vol. 89, no. 3, pp. 201–210, 2001, doi: 10.1161/hh1501.094396.

[84] T. P. Lozito and R. S. Tuan, “Mesenchymal stem cells inhibit both endogenous and exogenous MMPs via secreted TIMPs,” *J. Cell. Physiol.*, vol. 226, no. 2, pp. 385–396, 2011, doi: 10.1002/jcp.22344.

[85] F. yan Zhao *et al.*, “G-CSF Inhibits Pulmonary Fibrosis by Promoting BMSC Homing to the Lungs via SDF-1/CXCR4 Chemotaxis,” *Sci. Rep.*, vol. 10, no. 1, pp. 1–11, 2020, doi: 10.1038/s41598-020-65580-2.

[86] A. I. Caplan and J. E. Dennis, “Mesenchymal stem cells as trophic mediators,” *J. Cell. Biochem.*, vol. 98, no. 5, pp. 1076–1084, 2006, doi: 10.1002/jcb.20886.

[87] A. I. Caplan and D. Correa, “The MSC: An injury drugstore,” *Cell Stem Cell*, vol. 9, no. 1, pp. 11–15, 2011, doi: 10.1016/j.stem.2011.06.008.

[88] S. Dabrowska, A. Andrzejewska, M. Janowski, and B. Lukomska, “Immunomodulatory and Regenerative Effects of Mesenchymal Stem Cells and Extracellular Vesicles: Therapeutic Outlook for Inflammatory and Degenerative Diseases,” *Front. Immunol.*, vol. 11, no. February, 2021, doi: 10.3389/fimmu.2020.591065.

[89] O. El Atat *et al.*, “An evaluation of the stemness, paracrine, and tumorigenic characteristics of highly expanded, minimally passaged adipose-derived stem cells,” *PLoS One*, vol. 11, no. 9, pp. 1–22, 2016, doi: 10.1371/journal.pone.0162332.

[90] T. Kotani, R. Masutani, T. Suzuka, K. Oda, S. Makino, and M. Ii, “Anti-inflammatory and anti-fibrotic effects of intravenous adipose-derived stem cell transplantation in a mouse model of bleomycin-induced interstitial pneumonia,” *Sci. Rep.*, vol. 7, no. 1, pp. 1–10, 2017, doi: 10.1038/s41598-017-15022-3.

[91] X. Bai *et al.*, “Both cultured and freshly isolated adipose tissue-derived stem cells enhance cardiac function after acute myocardial infarction,” *Eur. Heart J.*, vol. 31, no. 4, pp. 489–501, 2010, doi: 10.1093/eurheartj/ehp568.

[92] T. M. Lee *et al.*, “Preconditioned adipose-derived stem cells ameliorate cardiac fibrosis by regulating macrophage polarization in infarcted rat hearts through the PI3K/STAT3

pathway," *Lab. Investig.*, vol. 99, no. 5, pp. 634–647, 2019, doi: 10.1038/s41374-018-0181-x.

[93] H. J. Joo, J. H. Kim, and S. J. Hong, "Adipose tissue-derived stem cells for myocardial regeneration," *Korean Circ. J.*, vol. 47, no. 2, pp. 151–159, 2017, doi: 10.4070/kcj.2016.0207.

[94] H. Hosseinkhani, M. Hosseinkhani, S. Hattori, R. Matsuoka, and N. Kawaguchi, "Micro and nano-scale in vitro 3D culture system for cardiac stem cells," *J. Biomed. Mater. Res. - Part A*, vol. 94, no. 1, pp. 1–8, 2010, doi: 10.1002/jbm.a.32676.

[95] J. H. Houtgraaf *et al.*, "First experience in humans using adipose tissue-derived regenerative cells in the treatment of patients with ST-segment elevation myocardial infarction," *J. Am. Coll. Cardiol.*, vol. 59, no. 5, pp. 539–540, 2012, doi: 10.1016/j.jacc.2011.09.065.

[96] E. C. Perin *et al.*, "Adipose-derived regenerative cells in patients with ischemic cardiomyopathy: The PRECISE Trial," *Am. Heart J.*, vol. 168, no. 1, pp. 88-95.e2, 2014, doi: 10.1016/j.ahj.2014.03.022.

[97] A. J. Kanelidis, C. Premer, J. Lopez, W. Balkan, and J. M. Hare, "Route of delivery modulates the efficacy of mesenchymal stem cell therapy for myocardial infarction: a meta-analysis of preclinical studies and clinical trials," *Circ. Res.*, vol. 120, no. 7, pp. 1139–1150, 2017, doi: 10.1161/CIRCRESAHA.116.309819.

[98] M. Hofmann *et al.*, "Monitoring of bone marrow cell homing into the infarcted human myocardium," *Circulation*, vol. 111, no. 17, pp. 2198–2202, 2005, doi: 10.1161/01.CIR.0000163546.27639.AA.

[99] J. A. Burdick, R. L. Mauck, and S. Gerecht, "To Serve and Protect: Hydrogels to Improve

Stem Cell-Based Therapies," *Cell Stem Cell*, vol. 18, no. 1, pp. 13–15, 2016, doi: 10.1016/j.stem.2015.12.004.

[100] D. L. Kraitchman *et al.*, "Dynamic imaging of allogeneic mesenchymal stem cells trafficking to myocardial infarction," *Circulation*, vol. 112, no. 10, pp. 1451–1461, 2005, doi: 10.1161/CIRCULATIONAHA.105.537480.

[101] A. S. Mao *et al.*, "Programmable microencapsulation for enhanced mesenchymal stem cell persistence and immunomodulation," *Proc. Natl. Acad. Sci. U. S. A.*, vol. 116, no. 31, pp. 15392–15397, 2019, doi: 10.1073/pnas.1819415116.

[102] R. Zhang *et al.*, "Particle-based artificial three-dimensional stem cell spheroids for revascularization of ischemic diseases," *Sci. Adv.*, vol. 6, no. 19, pp. 1–14, 2020, doi: 10.1126/sciadv.aaz8011.

[103] G. C. Gurtner, M. J. Callaghan, and M. T. Longaker, "Progress and potential for regenerative medicine," *Annu. Rev. Med.*, vol. 58, pp. 299–312, 2007, doi: 10.1146/annurev.med.58.082405.095329.

[104] P. B. Malafaya, G. A. Silva, and R. L. Reis, "Natural-origin polymers as carriers and scaffolds for biomolecules and cell delivery in tissue engineering applications," *Adv. Drug Deliv. Rev.*, vol. 59, no. 4–5, pp. 207–233, 2007, doi: 10.1016/j.addr.2007.03.012.

[105] B. Chevallay and D. Herbage, "Collagen-based biomaterials as 3D scaffold for cell cultures: Applications for tissue engineering and gene therapy," *Med. Biol. Eng. Comput.*, vol. 38, no. 2, pp. 211–218, 2000, doi: 10.1007/BF02344779.

[106] K. Wolf *et al.*, "Collagen-based cell migration models in vitro and in vivo," *Semin. Cell Dev. Biol.*, vol. 20, no. 8, pp. 931–941, 2009, doi: 10.1016/j.semcdb.2009.08.005.

[107] M. Meyer, "Processing of collagen based biomaterials and the resulting materials

properties," *Biomed. Eng. Online*, vol. 18, no. 1, pp. 1–74, 2019, doi: 10.1186/s12938-019-0647-0.

[108] C. Dong and Y. Lv, "Application of collagen scaffold in tissue engineering: Recent advances and new perspectives," *Polymers (Basel).*, vol. 8, no. 2, pp. 1–20, 2016, doi: 10.3390/polym8020042.

[109] A. Atala, F. Kurtis Kasper, and A. G. Mikos, "Engineering complex tissues," *Sci. Transl. Med.*, vol. 4, no. 160, pp. 1–11, 2012, doi: 10.1126/scitranslmed.3004890.

[110] T. Courtney, M. S. Sacks, J. Stankus, J. Guan, and W. R. Wagner, "Design and analysis of tissue engineering scaffolds that mimic soft tissue mechanical anisotropy," *Biomaterials*, vol. 27, no. 19, pp. 3631–3638, 2006, doi: 10.1016/j.biomaterials.2006.02.024.

[111] H. suk Yun, S. H. Kim, D. Khang, J. Choi, H. hoon Kim, and M. Kang, "Biomimetic component coating on 3D scaffolds using high bioactivity of mesoporous bioactive ceramics.," *Int. J. Nanomedicine*, vol. 6, pp. 2521–2531, 2011, doi: 10.2147/ijn.s25647.

[112] R. D. Levit *et al.*, "Cellular encapsulation enhances cardiac repair," *J. Am. Heart Assoc.*, vol. 2, no. 5, pp. 1–11, 2013, doi: 10.1161/JAHA.113.000367.

[113] R. J. Vagnozzi *et al.*, "An acute immune response underlies the benefit of cardiac stem cell therapy," *Nature*, vol. 577, no. 7790, pp. 405–409, 2020, doi: 10.1038/s41586-019-1802-2.

[114] Y. Shi *et al.*, "Immunoregulatory mechanisms of mesenchymal stem and stromal cells in inflammatory diseases," *Nat. Rev. Nephrol.*, vol. 14, no. 8, pp. 493–507, 2018, doi: 10.1038/s41581-018-0023-5.

[115] N. D. C. Noronha *et al.*, "Correction to: Priming approaches to improve the efficacy of

mesenchymal stromal cell-based therapies (Stem Cell Research and Therapy (2019) 10 (131) DOI: 10.1186/s13287-019-1224-y)," *Stem Cell Res. Ther.*, vol. 10, no. 1, pp. 1–21, 2019, doi: 10.1186/s13287-019-1259-0.

[116] A. Fuku *et al.*, "Evaluation of the Usefulness of Human Adipose-Derived Stem Cell Spheroids Formed Using SphereRing® and the Lethal Damage Sensitivity to Synovial Fluid In Vitro," *Cells*, vol. 11, no. 3, 2022, doi: 10.3390/cells11030337.

[117] L. Polonchuk *et al.*, "Cardiac spheroids as promising in vitro models to study the human heart microenvironment," *Sci. Rep.*, vol. 7, no. 1, pp. 1–12, 2017, doi: 10.1038/s41598-017-06385-8.

[118] S. Zhang, P. Liu, L. Chen, Y. Wang, Z. Wang, and B. Zhang, "The effects of spheroid formation of adipose-derived stem cells in a microgravity bioreactor on stemness properties and therapeutic potential," *Biomaterials*, vol. 41, pp. 15–25, 2015, doi: 10.1016/j.biomaterials.2014.11.019.

[119] D. Di Mascolo *et al.*, "Conformable hierarchically engineered polymeric micromeshes enabling combinatorial therapies in brain tumours," *Nat. Nanotechnol.*, vol. 16, no. 7, pp. 820–829, 2021, doi: 10.1038/s41565-021-00879-3.

[120] A. S. Go *et al.*, *Heart Disease and Stroke Statistics - 2014 Update: A report from the American Heart Association*, vol. 129, no. 3. 2014.

[121] M. F. Tenreiro, A. F. Louro, P. M. Alves, and M. Serra, "Next generation of heart regenerative therapies: progress and promise of cardiac tissue engineering," *npj Regen. Med.*, vol. 6, no. 1, 2021, doi: 10.1038/s41536-021-00140-4.

[122] O. Bergmann *et al.*, "Evidence for cardiomyocyte renewal in humans," *Science (80-.).*, vol. 324, no. 5923, pp. 98–102, 2009, doi: 10.1126/science.1164680.

[123] Y. M. Kook, S. Hwang, H. Kim, K. J. Rhee, K. Lee, and W. G. Koh, “Cardiovascular tissue regeneration system based on multiscale scaffolds comprising double-layered hydrogels and fibers,” *Sci. Rep.*, vol. 10, no. 1, pp. 1–12, 2020, doi: 10.1038/s41598-020-77187-8.

[124] S. Miyagawa *et al.*, “Long-term outcome of a dilated cardiomyopathy patient after mitral valve surgery combined with tissue-engineered myoblast sheets—report of a case,” *Surg. Case Reports*, vol. 4, no. 1, pp. 0–5, 2018, doi: 10.1186/s40792-018-0549-6.

[125] P. P. Zwetsloot *et al.*, “Cardiac stem cell treatment in myocardial infarction: A systematic review and meta-analysis of preclinical studies,” *Circ. Res.*, vol. 118, no. 8, pp. 1223–1232, 2016, doi: 10.1161/CIRCRESAHA.115.307676.

[126] B. A. Tompkins *et al.*, “Preclinical Studies of Stem Cell Therapy for Heart Disease,” *Circ. Res.*, vol. 122, no. 7, pp. 1006–1020, 2018, doi: 10.1161/CIRCRESAHA.117.312486.

[127] S. Bou-Ghannam, K. Kim, D. W. Grainger, and T. Okano, “3D cell sheet structure augments mesenchymal stem cell cytokine production,” *Sci. Rep.*, vol. 11, no. 1, pp. 1–11, 2021, doi: 10.1038/s41598-021-87571-7.

[128] A. El-Badawy *et al.*, “Adipose stem cells display higher regenerative capacities and more adaptable electro-kinetic properties compared to bone marrow-derived mesenchymal stromal cells,” *Sci. Rep.*, vol. 6, no. November, pp. 1–11, 2016, doi: 10.1038/srep37801.

[129] J. M. Karp and G. S. Leng Teo, “Mesenchymal Stem Cell Homing: The Devil Is in the Details,” *Cell Stem Cell*, vol. 4, no. 3, pp. 206–216, 2009, doi: 10.1016/j.stem.2009.02.001.

[130] S. P. Sevari, S. Ansari, and A. Moshaverinia, “A narrative overview of utilizing biomaterials to recapitulate the salient regenerative features of dental-derived mesenchymal stem cells,” *Int. J. Oral Sci.*, vol. 13, no. 1, 2021, doi: 10.1038/s41368-021-

00126-4.

[131] V. F. M. Segers and R. T. Lee, “Biomaterials to enhance stem cell function in the heart,” *Circ. Res.*, vol. 109, no. 8, pp. 910–922, 2011, doi: 10.1161/CIRCRESAHA.111.249052.

[132] M. Araña *et al.*, “Preparation and characterization of collagen-based ADSC-carrier sheets for cardiovascular application,” *Acta Biomater.*, vol. 9, no. 4, pp. 6075–6083, 2013, doi: 10.1016/j.actbio.2012.12.014.

[133] N. D. Kadir, Z. Yang, A. Hassan, V. Denslin, and E. H. Lee, “Electrospun fibers enhanced the paracrine signaling of mesenchymal stem cells for cartilage regeneration,” *Stem Cell Res. Ther.*, vol. 12, no. 1, pp. 1–17, 2021, doi: 10.1186/s13287-021-02137-8.

[134] N. Su, P. L. Gao, K. Wang, J. Y. Wang, Y. Zhong, and Y. Luo, “Fibrous scaffolds potentiate the paracrine function of mesenchymal stem cells: A new dimension in cell-material interaction,” *Biomaterials*, vol. 141, pp. 74–85, 2017, doi: 10.1016/j.biomaterials.2017.06.028.

[135] G. N. Yang, Z. Kopecki, D. Ph, and A. J. C. P. D, *Role of actin cytoskeleton in the regulation of epithelial cutaneous stem cells*. .

[136] V. A. Online and T. Pompe, “Cytoskeletal transition in patterned cells correlates with interfacial energy model,” pp. 2444–2452, 2014, doi: 10.1039/c3sm52424h.